Flow Boiling Heat Transfer and Pressure Drop Characteristics of a 45/55% by Weight Mixture of R32/R125

T. C. Villanueva, J. C. Chato, R. L. Shimon, N. M. DeGuzman, M. Ponchner,
K. A. Sweeney, N. L. Rhines, D. G. Allen, and T. T. Hershberger

ACRC TR-83 August 1995

For additional information:

Air Conditioning and Refrigeration Center
University of Illinois
Mechanical & Industrial Engineering Dept.
1206 West Green Street
Urbana, IL 61801

(217) 333-3115

Prepared as part of ACRC Project 37
Effect of Geometric Variables and R-22 Alternatives
on Refrigerant-Side Evaporation and Condensation
J. C. Chato, Principal Investigator

The Air Conditioning and Refrigeration Center was founded in 1988 with a grant from the estate of Richard W. Kritzer, the founder of Peerless of America Inc. A State of Illinois Technology Challenge Grant helped build the laboratory facilities. The ACRC receives continuing support from the Richard W. Kritzer Endowment and the National Science Foundation. The following organizations have also become sponsors of the Center.

Acustar Division of Chrysler
Amana Refrigeration, Inc.
Brazeway, Inc.
Carrier Corporation
Caterpillar, Inc.
Delphi Harrison Thermal Systems
E. I. du Pont de Nemours & Co.
Eaton Corporation
Electric Power Research Institute
Ford Motor Company
Frigidaire Company
General Electric Company
Lennox International, Inc.
Modine Manufacturing Co.
Peerless of America, Inc.
U. S. Army CERL
U. S. Environmental Protection Agency
Whirlpool Corporation

For additional information:

Air Conditioning & Refrigeration Center
Mechanical & Industrial Engineering Dept.
University of Illinois
1206 West Green Street
Urbana IL 61801

217 333 3115

FLOW BOILING HEAT TRANSFER AND PRESSURE DROP
CHARACTERISTICS OF A 45/55 % BY WEIGHT MIXTURE OF R32/R125

Tisha C. Villanueva, M.S.
Department of Mechanical and Industrial Engineering
University of Illinois at Urbana-Champaign, 1995
J.C. Chato, Advisor

ABSTRACT

This study investigates the heat transfer and pressure drop characteristics of a 45/55% by weight mixture of R32/R125. For mass fluxes above 150 x 10^3 lb_m/ft^2-h (200 kg/m^2-s) and heat fluxes below 6400 Btu/ft^2-h (20 kW/m^2), the experimental Nusselt number is dependent on both heat flux and quality. An increase in either of these qualities results in an increase in the Nusselt number. For mass fluxes below 150 x 10^3 lb_m/ft^2-h (200 kg/m^2-s), the Nusselt number is independent of quality. Pressure drop is dependent on heat flux and quality for the entire range of mass fluxes tested. The accuracy of several two-phase correlations in predicting the experimental data is examined. The Shah [1976] correlation underpredicts the experimental Nusselt number and this is attributed to an underestimation of the convective boiling contribution. The Jung and Radermacher [1989] correlation overpredicts the data. This is due, in part, to the absence of accurate surface tension data for the mixture. The Wattelet [1994] correlation predicts the experimental Nusselt number to within ±20%. The Sousa [1993] correlation predicts the experimental pressure drop to within ± 10%.

TABLE OF CONTENTS

Page

LIST OF TABLES vii

LIST OF FIGURES viii

NOMENCLATURE x

CHAPTER

1 Introduction 1

2 Literature Review 2
- 2.1 Flow Regimes 2
- 2.2 Heat Transfer Correlations for Pure Fluids 3
  - 2.2.1 The Shah Correlation 3
  - 2.2.2 The Jung and Radermacher Correlation 5
  - 2.2.3 The Wattelet Correlation 6
- 2.3 Pressure Drop 7
- 2.4 Mixtures 9
  - 2.4.1 Circumferential Temperature Distribution 9
  - 2.4.2 Nucleate Boiling Degradation 10
  - 2.4.3 Convective Boiling Degradation 11

3 Experimental Apparatus 16
- 3.1. Experimental Test Facility 16
  - 3.1.1 Refrigerant Loop 16
  - 3.1.2 Chiller system 17
  - 3.1.3 Test Section 18
  - 3.1.4 Data Acquisition System 19
- 3.2 Instrumentation 20
  - 3.2.1 Mass Flow Measurements 20
  - 3.2.2 Power Measurements 20
  - 3.2.3 Pressure Measurements 20
  - 3.2.4 Temperature Measurements 21

4 Experimental Procedures 25
- 4.1 Experimental Facility Operation 25
  - 4.1.1 System Preparation 25
  - 4.1.2 Data Collection Procedures 26
- 4.2 Data Reduction 26
- 4.3 Data Validation 29
- 4.4 Uncertainty Analysis 29
- 4.3 Test Matrix 30

5 Experimental Results 32
- 5.1 Heat Transfer Results 32
  - 5.1.1 Effects of Mass Flux, Heat Flux, and Quality 32
  - 5.1.2 Comparison with Previous Studies 33
  - 5.1.3 Comparisons with Correlations 34
- 5.2 Pressure Drop Results 35

6 Conclusions and Recommendations 48
6.1 Conclusions 48
6.2 Recommendations 49

REFERENCES 50

APPENDIX A Thermophysical Properties 53
APPENDIX B Experimental Data 55

LIST OF TABLES

Table		Page
4.1	Mean deviation of single phase correlations	29
4.2	Parameter uncertainties	30
4.3	Test Conditions	30
B.1	Experimental data	55

LIST OF FIGURES

Figure		Page
2.1	Flow regimes found during two-phase horizontal flow (Adapted from Dobson [1994])	13
2.2	Flow regime map based on visual observations (Adapted from Wattelet [1994])	14
2.3	Variation of the local heat transfer coefficient with quality in the stratified or wavy flow regimes (Adapted from Christoffersen [1993])	14
2.4	Variation of the local heat transfer coefficient with quality in the annular flow regime (Adapted Christoffersen [1993])	15
3.1	Experimental apparatus	22
3.2	Schematic of chiller system	22
3.3	Schematic of previous test section	23
3.4	Schematic of the new test section	23
3.5	Pressure tap	24
4.1	Experimental single-phase Nusselt number versus predicted single-phase Nusselt number	31
5.1	Experimental Nusselt number versus average quality at G=370 x 10^3 Btu/ft^2-h (500 kg/m^2-s)	36
5.2	Experimental Nusselt number versus average quality at G=220 x 10^3 Btu/ft^2-h (300 kg/m^2-s)	36
5.3	Experimental Nusselt number versus average quality at G=150 x 10^3 Btu/ft^2-h (200 kg/m^2-s)	37
5.4	Experimental Nusselt number versus average quality at G=75 x 10^3 Btu/ft^2-h (100 kg/m^2-s)	37
5.5	Experimental Nusselt number versus average quality at G=37 x 10^3 Btu/ft^2-h (50 kg/m^2-s)	38
5.6	Comparison of experimental Nusselt numbers to Christoffersen [1993] Nusselt numbers at G=370 x 10^3 Btu/ft^2-h (500 kg/m^2-s)	38
5.7	Comparison of experimental Nusselt numbers to Christoffersen [1993] Nusselt numbers at G=220 x 10^3 Btu/ft^2-h (300 kg/m^2-s)	39
5.8	Comparison of experimental Nusselt numbers to Christoffersen [1993] Nusselt numbers at G=150 x 10^3 Btu/ft^2-h (200 kg/m^2-s)	39
5.9	Experimental Nusselt number versus predicted Nusselt number for Shah correlation (DuPont property data)	40
5.10	Experimental Nusselt number versus predicted Nusselt number for Shah correlation (Ideal mixture properties)	40
5.11	Experimental Nusselt number versus predicted Nusselt number for Jung and Radermacher correlation (DuPont property data)	41

5.12 Experimental Nusselt number versus predicted Nusselt number for Jung and Radermacher correlation (Ideal mixture properties) 41
5.13 Experimental Nusselt number versus predicted Nusselt number for Wattelet correlation (DuPont property data) 42
5.14 Experimental Nusselt number versus predicted Nusselt number for Wattelet correlation (Ideal mixture properties) 42
5.15 Experimental pressure drop versus average quality at G=370 x 10^3 Btu/ft^2-h (500 kg/m^2-s) 43
5.16 Experimental pressure drop versus average quality at G=220 x 10^3 Btu/ft^2-h (300 kg/m^2-s) 43
5.17 Experimental pressure drop versus average quality at G=150 x 10^3 Btu/ft^2-h (200 kg/m^2-s) 44
5.18 Experimental pressure drop versus average quality at G=75 x 10^3 Btu/ft^2-h (100 kg/m^2-s) 44
5.19 Experimental pressure drop versus average quality at G=37 x 10^3 Btu/ft^2-h (50 kg/m^2-s) 45
5.20 Comparison of experimental pressure drop to Christoffersen [1993] pressure drop at G=370 x 10^3 Btu/ft^2-h (500 kg/m^2-s) 45
5.21 Comparison of experimental pressure drop to Christoffersen [1993] pressure drop at G=220 x 10^3 Btu/ft^2-h (300 kg/m^2-s) 46
5.22 Comparison of experimental pressure drop to Christoffersen [1993] pressure drop at G=150 x 10^3 Btu/ft^2-h (200 kg/m^2-s) 46
5.23 Experimental pressure drop versus pressure drop predicted by the Sousa correlation 47

NOMENCLATURE

A	Area	
A_s	Surface area	
Bo	Boiling number	$=\frac{q''}{Gi_{lv}}$
c_{p_l}	Liquid specific heat	
Co	Convection number	$=\left(\frac{1-x}{x}\right)^{0.8}\left(\frac{\rho_v}{\rho_l}\right)^{0.5}$
d_i	Inner diameter	
$\frac{dp}{dz}$	Pressure gradient	
$(-dp/dz)_{acceleration}$	Acceleration pressure gradient	
$(-dp/dz)_{friction}$	Frictional pressure gradient	
$(dP/dz)_l$	Liquid alone pressure gradient	
$(dP/dz)_{TPf}$	Two-phase frictional pressure gradient	
$(dP/dz)_v$	Vapor alone pressure gradient	
D_i	Inner diameter	
D_b	Bubble departure diameter	
f_l	Friction factor	
F	Two-phase multiplier for heat transfer	
F_p	Two-phase enhancement factor	
Fr_l	Liquid Froude number	$=\frac{G^2}{\rho_l^2 gD}$
g	Acceleration of gravity	
G	Mass flux	
h	Heat transfer coefficient	
h_{cb}	Convective boiling heat transfer coefficient	$=Fh_l$
h_I	Ideal heat transfer coefficient	

h_l	Single phase heat transfer coefficient	
h_{nb}	Nucleate boiling heat transfer coefficient	
h_{TP}	Two-phase heat transfer coefficient	
h_1	Heat transfer coefficient of more volatile component	
h_2	Heat transfer coefficient of less volatile component	
i_l	Saturated liquid enthalpy	
i_{lv}	Latent heat of vaporization	
$i_{preheater,in}$	Enthalpy of refrigerant entering the preheater	
$i_{preheater,out}$	Enthalpy of refrigerant leaving the preheater	
$i_{test\ section,out}$	Enthalpy of refrigerant leaving the test section	
i_v	Saturated vapor enthalpy	
k_l	Liquid thermal conductivity	
K	Empirical constant	
L_{HX}	Heat transfer length	
$\dot{m}$	Mass flow rate	
$\dot{m}_l$	Liquid mass flow rate	
$\dot{m}_v$	Vapor mass flow rate	
M	Molecular weight	
n	Exponent	
N	Variable used in the Shah and Jung and Radermacher correlations	
Nu	Two-phase liquid Nusselt number	$= \frac{h_{TP}D}{k_l}$
P	Pressure	
P_l	Wetted perimeter of liquid phase	
P_r	Reduced pressure	$= \frac{P_{sat}}{P_{crit}}$
P_v	Wetted perimeter of vapor phase	
Pr_l	Liquid Prandtl number	$= \frac{\mu_l c_{p_l}}{k_l}$

q	Heat input rate	
q''	Heat flux	
$q_{preheater}$	Electrical heat input rate to the preheater	
$\dot{Q}_{TS}$	Heat input into the test section	
R	Bubble radius	
R	Convection reduction parameter	
Re_l	Liquid alone Reynolds number	$= \frac{GD(1-x)}{\mu_l}$
T	Temperature	
T_b	Bulk fluid temperature	
T_i	New temperature of liquid surrounding the wall	
$T_{preheater,in}$	Refrigerant temperature at preheater inlet	
$T_{preheater,out}$	Refrigerant temperature at preheater outlet	
T_s	Surface temperature	
T_{sat}	Saturation temperature	
$T_{test\,section,in}$	Refrigerant temperature at test section inlet	
$T_{test\,section,out}$	Refrigerant temperature at test section outlet	
$\overline{T}_b$	Average bulk fluid temperature	
$\overline{T}_s$	Average surface temperature	
V_l	Liquid velocity	
V_v	Vapor velocity	
x	Quality	
x_{avg}	Average quality	
x_i	Inlet quality	
x_o	Outlet quality	
$\tilde{x}_1$	Mole fraction of more volatile component	
$\tilde{x}_2$	Mole fraction of less volatile component	
$\tilde{x}_{1,l}$	Liquid phase mole fraction of more volatile component	

$\tilde{x}_{l,v}$	Vapor phase mole fraction of more volatile component
X	Lockhart-Martinelli parameter $X = \sqrt{\frac{(dp/dz)_l}{(dp/dz)_v}}$
X_{tt}	Turbulent-Turbulent Lockhart-Martinelli parameter $= \left(\frac{1-x}{x}\right)^{0.9}\left(\frac{\rho_v}{\rho_l}\right)^{0.5}\left(\frac{\mu_l}{\mu_v}\right)^{0.1}$
α_i	Inlet void fraction
α_o	Outlet void fraction
β	Contact angle
δd_i	Uncertainty in the diameter measurement
δh	Uncertainty in the heat transfer coefficient
δL_{HX}	Uncertainty in the heat transfer length
$\delta \dot{Q}_{TS}$	Uncertainty in the heat input to the test section
$\delta \overline{T}_b$	Uncertainty in the average bulk fluid temperature
$\delta \overline{T}_s$	Uncertainty in the average surface temperature
$\delta h/\delta d_i$	Sensitivity of heat transfer coefficient with respect to diameter
$\delta h/\delta L_{HX}$	Sensitivity of heat transfer coefficient with respect to heat transfer length
$\delta h/\delta \dot{Q}_{TS}$	Sensitivity of heat transfer coefficient with respect to the heat input
$\delta h/\delta \overline{T}_b$	Sensitivity of heat transfer coefficient with respect to the average bulk fluid temperature
$\delta h/\delta \overline{T}_s$	Sensitivity of heat transfer coefficient with respect to the average surface temperature
ΔP	Pressure drop
ΔP_a	Acceleration pressure drop
ΔP_f	Friction pressure drop
ΔP_g	Gravitational pressure drop
ΔP_l	Single-phase liquid alone pressure drop
ΔP_{total}	Total pressure drop

ΔT_I	Ideal wall superheat
ΔT_m	Mixture wall superheat
ΔT_1	Wall superheat of more volatile component
ΔT_2	Wall superheat of less volatile component
μ_l	Liquid viscosity
μ_v	Vapor viscosity
ρ_l	Liquid density
ρ_v	Vapor density
σ	Surface tension
τ_w	Shear stress at the wall
ϕ	Two-phase frictional multiplier
ϕ_l	Two-phase frictional multiplier based on pressure gradient for liquid alone flow
ϕ_v	Two-phase frictional multiplier based on pressure gradient for vapor alone flow
Ψ	Multiplier used in the Shah correlation
Ψ_{bs}	Bubble suppression multiplier used in the Shah correlation
Ψ_{cb}	Convective boiling multiplier used in the Shah correlation
Ψ_{nb}	Nucleate boiling multiplier used in the Shah correlation

CHAPTER 1
Introduction

For the past several years, many different refrigerants have been studied in order to find a possible replacement for R12. Testing with R32 has shown that its heat transfer coefficients are much higher than R12 under the same conditions. Unfortunately, R32 is flammable.

In order to take advantage of the heat transfer properties of R32 and reduce the flammability of the refrigerant, various mixtures using R32 as one of the components have been developed. Most of these refrigerants are zeotropes. Zeotropes are fluids which, for a given pressure, do not have the same saturation temperature for the vapor phase as the liquid phase . This is called the temperature glide. Zeotropes also have a tendency to change composition whenever refrigerant is added or removed from the system. Therefore, testing with these fluids is very difficult.

Fortunately, for certain combinations of refrigerants, certain compositions result in the formation of an azeotrope. An azeotrope is a mixture that has the characteristics of a pure fluid. There is no temperature glide and it's composition does not change under most conditions. The present study investigates the properties of a 45/55 % by weight mixture of R32/R125. This mixture is a near azeotrope. Since it has a very small glide, it is treated as a pure fluid in this study.

The heat transfer and pressure drop characteristics during evaporation are presented. In addition, comparisons between the experimental data and previous R32/R125 are made. Finally, the accuracy of several two-phase correlations in predicting the experimental data is examined.

The two-phase correlations used in this study are described in detail in Chapter 2. That chapter also contains information on the flow regimes present during two-phase flow in an evaporator as well as an account of mixture behavior. This is followed by a description of the experimental apparatus in Chapter 3. Chapter 4 outlines the procedures required to operate the system, the variables controlled during the experiments, and the test matrix used in the study. Chapter 5 describes all the experimental data gathered during the investigation and presents possible explanations to the refrigerant's behavior. Finally, Chapter 6 summarizes the conclusions and proposes areas for new research.

CHAPTER 2
Literature Review

This chapter presents related work performed by other investigators as well as relevant background information necessary in the discussion of their results. In the first section, the different flow regimes found in horizontal two phase flow are described. This is followed by a discussion of different pure fluid heat transfer and pressure drop correlations available in literature. Finally, refrigerant mixture behavior is outlined and possible explanations of its deviation from pure refrigerant characteristics are given.

2.1 Flow Regimes

Since the heat transfer coefficient is greatly affected by the flow regime present in the refrigerant, identifying and characterizing each regime is important. In the beginning of the evaporation process, bubbles start to form in the subcooled liquid. These bubbles float to the top since they are much lighter than the surrounding refrigerant. As the fluid gains more heat, it moves from this phase, which is called bubble flow, to plug flow. This regime is characterized by pockets of vapor which stay at the top of the tube and increased liquid and vapor velocities.

As evaporation continues, the fluid changes from plug flow into either stratified flow or wavy flow. This transformation is governed by the velocities of the liquid and vapor components which, in turn, are controlled by the mass flux. At low mass fluxes, the liquid and vapor are moving relatively slowly and two distinct layers are formed. This is called stratified flow. Alternatively, at higher mass fluxes, both the liquid and vapor have high velocities. As the velocity of the vapor becomes greater than that of the liquid, sharp gradients arise which cause waves in the liquid to form. This regime, which is called wavy or wavy-annular flow, is characterized by waves which appear in the liquid-vapor interface.

At higher qualities and higher mass fluxes, the liquid refrigerant forms a layer which coats the entire tube wall and surrounds a vapor core. At moderately high mass fluxes, gravity tends to pull the liquid from the walls and cause it to pool at the bottom of the tube. Thus, the liquid layer is thicker on the bottom than on the top. At very high mass fluxes, however, strong Reynolds stresses and shear overcome this force and the liquid layer has a uniform thickness [Carey, 1992]. In this flow regime, which is called annular flow, the heat transfer coefficient of the two-phase flow is at its highest. Since the thermal conductivity of liquid is typically higher than that of vapor, the most heat transfer takes

place when the most liquid is in contact with the tube wall. This occurs during annular flow.

As the quality increases even more, the high vapor velocity causes waves to form at the liquid-vapor interface. Liquid is entrained in the vapor core in the form of droplets and eventually the entire liquid layer disappears. This is mist flow. Following mist flow is dry out. This occurs when all the liquid has been vaporized and only vapor is left. Figure 2.1 shows a visual representation of each flow regime. Figure 2.2 indicates the mass flux and quality at which each regime is likely to occur.

2.2 Heat Transfer Correlations for Pure Fluids

For an evaporator, heat transfer occurs through the following mechanisms: nucleate boiling and convective boiling. Nucleate boiling is characterized by heat transfer at the tube wall which results in the formation and growth of bubbles. Nucleate boiling dominates in conditions of low mass flux and low quality - the stratified and wavy regimes. It is also very dependent on heat flux, increasing as the heat flux increases, as shown in figure 2.3.

In contrast to nucleate boiling, convective boiling takes place at the liquid-vapor interface. This type of heat transfer is highly dependent on the velocity of the vapor present in the flow, thus it is greatly influenced by quality. This dependence is shown in figure 2.4. Convective boiling is the dominant mode of heat transfer in the wavy-annular and annular regimes, but these flows also exhibit some nucleate boiling heat transfer.

The interaction between the two types of evaporative heat transfer is not clearly established. Different correlations take different approaches in combining the two modes and deriving a single formula that predicts the heat transfer coefficient for all the flow regimes. In the following sections, three different heat transfer coefficients developed for pure fluids are reviewed and the differences in their approaches are discussed.

2.2.1 The Shah Correlation

Shah [1976] based his two-phase heat transfer correlation on several databases gathered from literature. For his correlation, Shah defined the following four flow regimes: the bubble suppression regime, the pure convection regime, the pure nucleate boiling regime, and the convective boiling with partly dry surface regime. At low mass fluxes and low qualities, nucleate boiling dominates and the flow is in the pure nucleate boiling regime. As the quality increases, nucleate boiling is suppressed and nucleate boiling and convective boiling occur simultaneously. This is the bubble suppression regime. As the mass flux and quality are increased further, convective boiling dominants and the flow is in the pure convection regime. Finally, stratified flow is taken into account

by the convective boiling with partly dry surface regime. The tube wall is not completely wet due to the stratification of the liquid and vapor layers.

Shah uses criteria based on two dimensionless numbers to determine the appropriate flow regime for the given conditions. These dimensionless numbers are the convection number, Co, and the liquid Froude number, Fr_l. These parameters are defined as follows:

$$Co = \left(\frac{1}{x} - 1\right)^{0.8} \left(\frac{\rho_v}{\rho_l}\right)^{0.5} \tag{2.1}$$

$$Fr_l = \frac{G^2}{\rho_l^2 g D_i} \tag{2.2}$$

Once the flow regime is decided, two different heat transfer correlations are calculated and the larger of the two is used. To calculate the heat transfer coefficient, the correlation uses the Dittus-Boelter single phase correlation and a multiplier. The single phase heat transfer coefficient, h_l, the two-phase heat transfer coefficient, h_{TP}, and the multiplier, Ψ, are defined as follows:

$$h_l = 0.023 \frac{k_l}{D_i} Re_l^{0.8} Pr_l^{0.4} \tag{2.3}$$

$$h_{TP} = \Psi h_l \tag{2.4}$$

where

For $Fr_l > 0.04$, $N = Co$; else $N = 0.38\ Fr_l^{-0.3}\ Co$ (2.5a)

For $N > 1$

$\Psi_{nb} = 230 Bo^{0.5}$, $Bo > 0.3 \times 10^{-4}$ (2.5b)

$\Psi_{nb} = 1 + 46 Bo^{0.5}$, $Bo < 0.3 \times 10^{-4}$ (2.5c)

$\Psi_{cb} = \frac{1.8}{N^{0.8}}$, for all N (2.5d)

Ψ is the larger of Ψ_{nb} and Ψ_{cb} (2.5e)

For $0.1 < N \leq 1.0$

$\Psi_{bs} = F Bo^{0.5} \exp(2.74 N^{-0.1})$ (2.5f)

where $F=14.7$ for $Bo \geq 11 \times 10^{-4}$; else $F=15.43$ (2.5g)

Ψ is the larger of Ψ_{bs} and Ψ_{cb} (2.5h)

For $N \leq 0.1$

$$\Psi_{bs} = FBo^{0.5}\exp\left(2.47N^{-0.15}\right) \tag{2.5i}$$

Ψ is the larger of Ψ_{bs} and Ψ_{cb} (2.5j)

2.2.2 The Jung and Radermacher Correlation

Unlike Shah's "greater of the two" method, Jung and Radermacher [1989] employ an additive model of the following form:

$$h_{TP} = h_{nb} + h_{cb} \tag{2.6}$$

In the above equation, the nucleate boiling contribution, h_{nb}, is a function of Stephen and Abdelsalam's [1980] nucleate pool boiling heat transfer correlation, h_{SA}, and a boiling suppression factor, N. These variables are defined in the following equations:

$$h_{nb} = Nh_{SA} \tag{2.7}$$

$$h_{SA} = 207\frac{k_l}{D_b}\left(\frac{qD_b}{k_l T_{sat}}\right)^{0.745}\left(\frac{\rho_v}{\rho_l}\right)^{0.581} Pr_l^{0.533} \tag{2.8}$$

where

$$D_b = 0.0146\beta\left[\frac{2\sigma}{g(\rho_l - \rho_v)}\right]^{0.5} \tag{2.9}$$

$$N = 4048X_{tt}^{1.22}Bo^{1.13} \qquad \text{for } X_{tt} \leq 1 \tag{2.10a}$$

$$N = 2.0 - 0.1X_{tt}^{-0.28}Bo^{-0.33} \qquad \text{for } 1 < X_{tt} \leq 5 \tag{2.10b}$$

The variable β, which is found in equation 2.9, represents the contact angle between the liquid-vapor interface and the solid surface. It has a value of 35°. The variable X_{tt} is the Lockhart-Martinelli parameter and is defined in greater detail in section 2.3.

The convective boiling contribution to the heat transfer coefficient, h_{cb}, has a form similar to that of nucleate boiling. It is a function of a single phase heat transfer coefficient, h_l, which is defined by equation 2.3, and a two-phase enhancement factor, F. These parameters are defined in the following equations:

$$h_{cb} = F_p h_l \tag{2.11}$$

$$F = 2.37\left(0.29 + \frac{1}{X_{tt}}\right)^{0.85} \tag{2.12}$$

2.2.3 The Wattelet Correlation

Wattelet [1994] uses an asymptotic model proposed by Kutateladze [1961] to combine the nucleate boiling and convective boiling modes of heat transfer. This model is of the form

$$h_{TP} = \left[h_{nb}^{n} + h_{cb}^{n}\right]^{\frac{1}{n}} \tag{2.13}$$

where

$$n=2.5 \tag{2.14}$$

Unlike the Jung and Radermacher correlation, this one does not require correction factors. The form of the equation takes into account any nucleate or convective boiling suppression. Interestingly, as n approaches infinity, the equation takes the form of Shah's "greater of the two" equation and if n equals 1, the correlation becomes an additive model of the form of the Jung and Radermacher equation.

The nucleate boiling contribution, h_{nb}, is given by Cooper's [1984] pool boiling correlation. This correlation is based on reduced pressure, P_r, molecular weight, M, and heat flux, q". This correlation was selected over the Stephan and Abdelsalam correlation because it does not use surface tension, which is not always available for certain refrigerants. The nucleate boiling contribution is defined as follows:

$$h_{nb} = 55q''^{0.67} M^{-0.5} P_r^{0.12}\left[-\log_{10} P_r\right]^{-0.55} \tag{2.15}$$

The convective boiling contribution is a function of the single phase heat transfer coefficient defined in equation 2.3, a two phase enhancement factor, F, and a Froude number dependent term, R, that takes into account heat transfer decreases at lower Reynolds number flows. These variables are defined as follows:

$$h_{cb} = Fh_l R \tag{2.16}$$

$$F = 1 + 1.925 X_{tt}^{-0.83} \tag{2.17}$$

$$R = 1.32 Fr_l^{0.2} \qquad \text{for } Fr_l \le 0.25 \qquad (2.18a)$$

$$R = 1 \qquad \text{for } Fr_l \ge 0.25 \qquad (2.18b)$$

2.3 Pressure Drop

Total pressure drop in a duct, ΔP_{total}, consists of the following components: pressure drop due to friction, ΔP_f, pressure drop due to change in momentum, ΔP_a, and pressure drop due to gravity, ΔP_g. For horizontal flow, however, the gravity term is ignored and the total pressure is given by the equation:

$$\Delta P_{total} = \Delta P_f + \Delta P_a \qquad (2.19)$$

Using the one-dimensional form of continuity and the momentum equations and assuming constant properties, steady state, and incompressible flow, the following equation for total pressure drop is derived [Wattelet, 1994]:

$$\left(-\frac{dp}{dz}\right) = \left[(\tau_w)_v P_v + (\tau_w)_l P_l\right] + \frac{1}{A}\frac{d}{dz}\left[\dot{m}_v V_v + \dot{m}_l V_l\right] \qquad (2.20)$$

where

$$\left(-\frac{dp}{dz}\right)_{friction} = (\tau_w)_v P_v + (\tau_w)_l P_l \qquad (2.21)$$

$$\left(-\frac{dp}{dz}\right)_{acceleration} = \frac{1}{A}\frac{d}{dz}\left[\dot{m}_v V_v + \dot{m}_l V_l\right] \qquad (2.22)$$

By integrating equation 2.22, applying continuity and the definition of void fraction, α, the acceleration pressure drop can be written in the following form:

$$-\Delta P_a = G^2\left\{\left[\frac{x_o^2}{\rho_v \alpha_o} + \frac{(1-x_o)^2}{\rho_l(1-\alpha_o)}\right] - \left[\frac{x_i^2}{\rho_v \alpha_i} + \frac{(1-x_i)^2}{\rho_l(1-\alpha_i)}\right]\right\} \qquad (2.23)$$

Void fraction, α, is defined by Zivi [1964] as:

$$\alpha = \frac{1}{1+\left(\frac{1-x}{x}\right)\left(\frac{\rho_v}{\rho_l}\right)^{0.67}} \tag{2.24}$$

As can be seen from the previous equations, the acceleration pressure drop is governed by the densities of the liquid and vapor components, the quality at the inlet and outlet of the tube, and the mass flux. The frictional pressure drop is also dependent on these factors as well as the viscosities. Lockhart and Martinelli [1947] proposed that the two-phase frictional pressure drop could be related to the single-phase frictional pressure drop by means of a two-phase multiplier, ϕ^2. This variable is defined as follows:

$$\phi_l^2 = \frac{(dP/dz)_{TPf}}{(dP/dz)_l} \tag{2.25}$$

$$\phi_v^2 = \frac{(dP/dz)_{TPf}}{(dP/dz)_v} \tag{2.26}$$

The subscript l refers to the two-phase pressure gradient calculated based on the liquid mass flow and the subscript v refers to quantities based on the vapor mass flow. Lockhart and Martinelli also proposed that the two-phase pressure drop falls between the pressure drop of pure liquid and pure vapor flow. Therefore, they defined a parameter, X, as the ratio of the pressure gradient of pure liquid flow to pure vapor flow. This is shown in the following equation:

$$X = \sqrt{\frac{\phi_v^2}{\phi_l^2}} = \sqrt{\frac{(dP/dz)_l}{(dP/dz)_v}} \tag{2.27}$$

For turbulent liquid and turbulent vapor flow, this parameter reduces to the form:

$$X_{tt} = \left(\frac{1-x}{x}\right)^{0.9}\left(\frac{\rho_v}{\rho_l}\right)^{0.5}\left(\frac{\mu_l}{\mu_l}\right)^{0.1} \tag{2.28}$$

Sousa [1992] used the Lockhart-Martinelli parameter to develop a two-phase multiplier in his frictional pressure drop correlation. This correlation uses the two-phase multiplier and the single phase pressure drop, ΔP_l. The correlation is as follows:

$$\Delta P_f = \Delta P_l \phi_l^2 \tag{2.29}$$

where

$$\Delta P_l = \frac{2 f_l G^2 (1-x)^2 L}{\rho_l D_i} \tag{2.30}$$

$$f_l = \frac{0.079}{Re_l^{0.25}} \tag{2.31}$$

$$\phi_l^2 = 1.376 + C_1 X_{tt}^{-C_2} \tag{2.32}$$

$$C_1 = 4.172 + 5.48 Fr_l - 1.564 Fr_l^2, \quad \text{for } 0 < Fr_l \le 0.7 \tag{2.33a}$$
$$C_2 = 1.773 - 0.169 Fr_l$$

$$C_1 = 7.242, \quad \text{for } Fr_l > 0.7 \tag{2.33b}$$
$$C_2 = 1.655$$

2.4 Mixtures

In the first part of this section, the difference in the circumferential temperature distribution between pure refrigerants and refrigerant mixtures is discussed. Not only does the temperature distribution of certain mixtures differ from that of pure fluid, they also display a decreased heat transfer coefficient. Possible explanations of this are given in sections 2.4.2 and 2.4.3. Sections 2.4.2 deals mainly with nucleate boiling suppression while section 2.4.3 focuses on the convective boiling contribution.

2.4.1 Circumferential Temperature Distribution

For pure fluids in annular flow, the liquid layer is slightly thicker on the bottom of the tube. This is due to gravity pulling the refrigerant toward the tube bottom. Since there is less resistance at the top of the tube, the heat transfer coefficient is higher at that location [Ross, Radermacher, Di Marzo, and Didion; 1987]. From this information, and assuming constant heat flux and saturation temperature, it is deduced that the temperature at the top of the tube is less than that at the bottom.

For certain refrigerant mixtures, however, the opposite is true. The liquid layer is also slightly thicker on the bottom than on the top. This is partly due to gravity but it is also attributed to the difference in volatility between the different components. Since the liquid layer is thicker on the bottom, there is a greater amount of the more volatile

component present at that location. The volatile component is the refrigerant with the lower normal boiling point. The volatile component in the thin layer at the top of the tube is soon boiled off and the temperature increases. The increase in temperature is followed by a decrease in the heat transfer coefficient. Jung, McLinden, Radermacher, and Didion [1989] observed this phenomena in experiments with mixtures of R22/R114. However, experiments with R12/R152a did not show this behavior. The mixture acted like a pure fluid. This discrepancy is explained by the difference in the volatility between the components. The difference in the normal boiling point of R22 and R114 is 80 °F (44.5°C) while the difference between R12 and R152a is only 9 °F (5 °C). For a mixture, the circumferential temperature difference is dependent on the volatility of its components.

2.4.2 Nucleate Boiling Degradation

In nucleate boiling, heat transfer that occurs through the formation, or nucleation, of bubbles on the tube wall. A sufficient wall superheat, which is defined as the difference between the wall temperature, T_w, and the saturation temperature of the bulk fluid, T_b, must be present in order to initiate nucleation. For mixtures, bubbles depart from the tube surface containing mostly the more volatile component. The boiling boundary layer is stripped of the more volatile component and the mole fraction, which is based on the more volatile component, decreases below that of the bulk fluid. As a result, the temperature of the local fluid is raised [Unal, 1986]. The wall superheat is no longer given by $(T_w - T_b)$ but by $(T_w - T_i)$. The new variable T_i represents the new temperature of the liquid surrounding the wall [Jung and Radermacher, 1993].

Thome [1983] proposes that this rise in local boiling point of the liquid surrounding the wall, ΔT_{bp}, can be determined from knowing only the phase equilibrium diagram of the mixture at the pressure of interest. This method uses a ratio of the heat transfer coefficient, h, to the ideal heat transfer coefficient, h_I, and a ratio of the ideal wall superheat, ΔT_I, to the actual wall superheat, ΔT_m. The equation is as follows:

$$\frac{h}{h_I} = \frac{\Delta T_I}{\Delta T_m} = \frac{\Delta T_I}{\Delta T_I + \Delta T_{bp}} \tag{2.34}$$

The ideal heat transfer coefficient is a function of the mole fractions and the heat transfer coefficients of the pure components. It is given by the following formula:

$$h_I = \frac{1}{(\tilde{x}_1/h_1) + (\tilde{x}_2/h_2)} \tag{2.35}$$

The ideal wall superheat is derived using the ideal mixing law

$$\Delta T_I = \tilde{x}_1 \Delta T_1 + \tilde{x}_2 \Delta T_2 \tag{2.36}$$

The previous equations are applicable to pool boiling. Another correlation used to predict the wall superheat during nucleate pool boiling is from Stephan and Korner [Unal, 1986]. This equation uses the variables K, $\tilde{x}_{l,l}$, and $\tilde{x}_{l,v}$ which represent an empirical constant that is different for every binary mixture, the mole fraction of liquid for the volatile component, and the mole fraction of vapor for the volatile component, respectively. It is as follows:

$$\frac{\Delta T_m}{\Delta T_I} = \left[1 + K\left|\tilde{x}_{l,v} - \tilde{x}_{l,l}\right|\left(0.88 + 0.12x10^{-5}P\right)\right] \tag{2.37}$$

In experiments, the temperatures measured are the bulk fluid temperature and the wall temperature. These are the temperatures used in calculating the heat transfer coefficient. However, if the boiling layer temperature, T_i, is much higher than the bulk fluid temperature, the temperature difference used in the heat transfer calculations is artificially high and gives a heat transfer coefficient that is too low. This could account for the degradation found in nucleate boiling contribution. Kedzierski, Kim, and Didion [1992] proposes that most of the decrease is caused by this phenomena.

Other investigators, however, attribute the decrease to other sources. Sardesai, Shock, and Butterworth [1982] agrees that the increase in the local fluid temperature contributes to the degradation in the heat transfer coefficient. An overestimation of the wall superheat causes an overestimation of the bubble growth rate. If the bubble growth rate is decreased, so is the bubble departure diameter. It is the combination of slower growing bubbles and smaller departure sizes that causes the decrease in the heat transfer coefficient. For an azeotrope, however, the bubble departure radius is the same as that of a pure substance [Jung et al. 1989]. Therefore, for an azeotrope, any decrease in the nucleate boiling contribution can only be due to an overestimation of the wall superheat.

2.4.3 Convective Boiling Degradation

According to Kedzierski et al. [1992], as the mixture evaporates, the bulk fluid is stripped of the more volatile component and the mass fraction of the more volatile component of the mixture is reduced. The liquid layer at the top of the tube is thinner than

that at the bottom and most of the volatile component is soon boiled off. The mass fraction of the volatile component at the top of the tube is less than that at the bottom and this introduces concentration gradients. These gradients cause an error in the temperature measurement. The measured temperature, which is the saturation temperature, is less than the temperature at the liquid vapor interface. An artificially high temperature difference is used to calculated the heat transfer coefficient, as in the case of nucleate boiling.

Kedzierski et al. [1992] also states that mass transfer contributes to the decrease in the heat transfer coefficient. Mass transfer affects the magnitudes of the concentration gradients and this, in turn, affects the temperature distribution in the flow. Ross et al. [1987] attributes the decrease in the convective boiling portion to the following: increased turbulence at the bottom of the tube, nucleate boiling present only at the bottom of the tube, flow pattern differences between mixtures and pure fluids, departure from nucleate boiling events, and different concentrations at the top and bottom of the tube. Jung and Radermacher [1993] propose that changes in several refrigerant properties cause the decrease in the heat transfer coefficient. As refrigerants are mixed, liquid thermal conductivity decreases while the liquid viscosity increases. High heat transfer coefficients are associated with high values of liquid thermal conductivity and low values of liquid viscosity. High thermal conductivity promotes the transfer of heat through conduction and low liquid viscosity means less resistance to heat transfer.

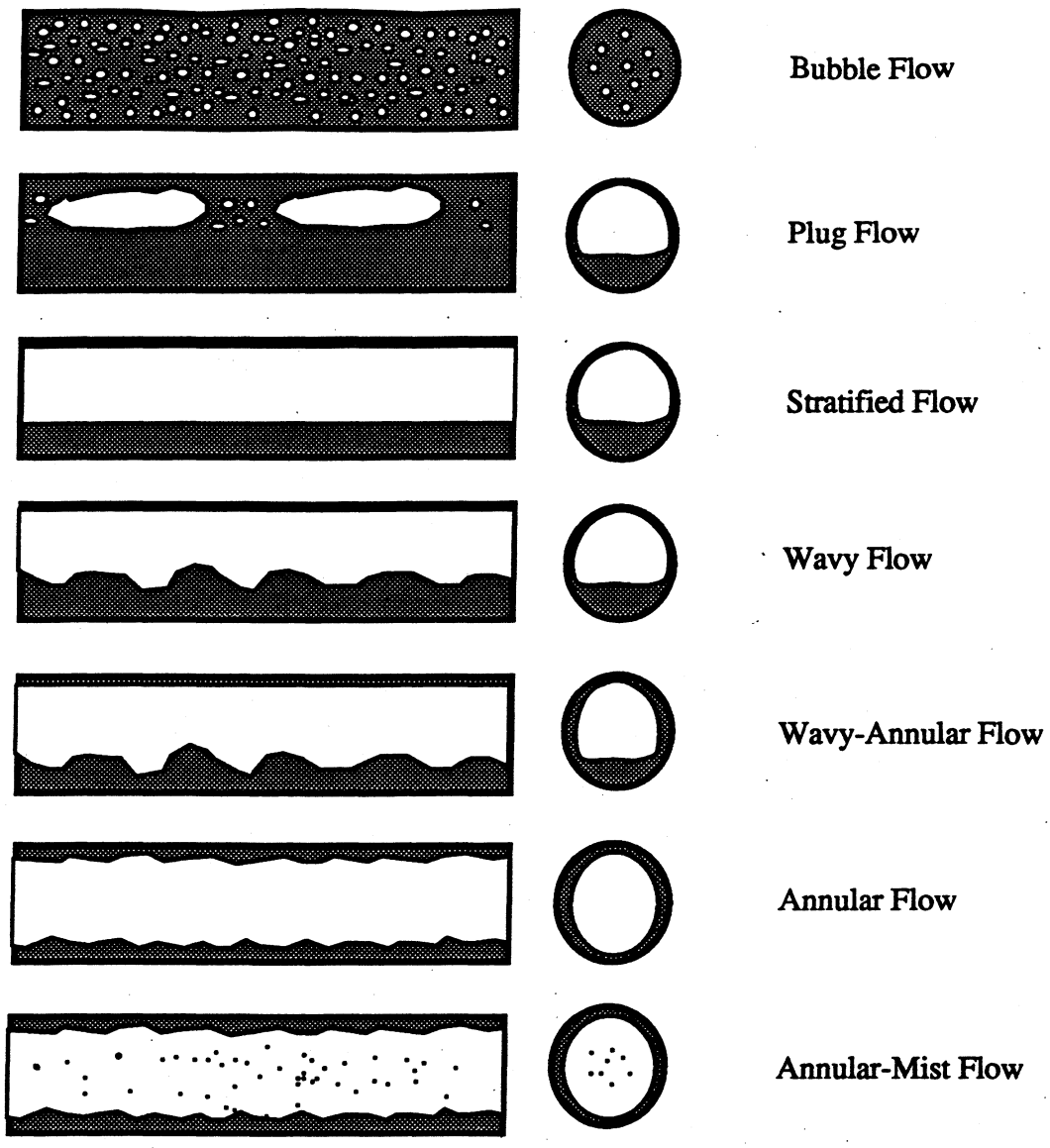

Figure 2.1 Flow regimes found during two-phase horizontal flow (Adapted from Dobson [1994])

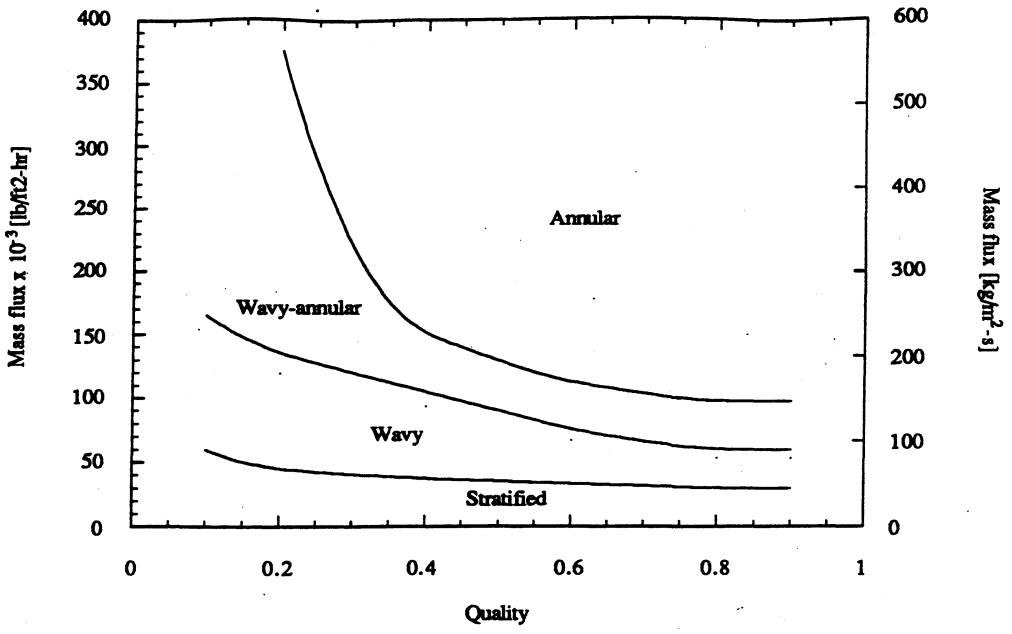

Figure 2.2 Flow regime map based on visual observations (Adapted from Wattelet [1994])

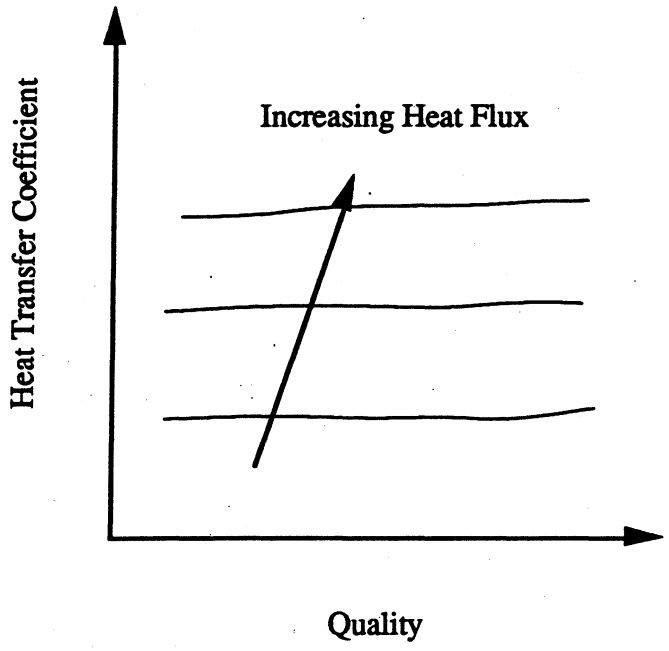

Figure 2.3 Variation of the local heat transfer coefficient with quality in the stratified or wavy flow regimes (Adapted from Christoffersen [1993])

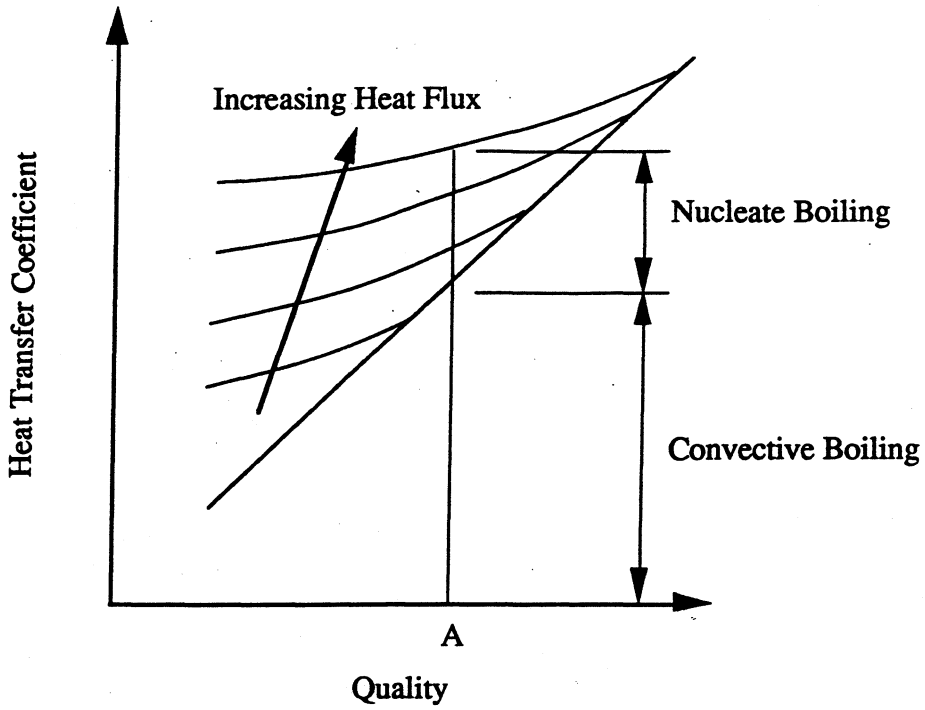

Figure 2.4 Variation of the local heat transfer coefficient with quality in the annular flow regime (Adapted from Christoffersen [1993])

CHAPTER 3
Experimental Apparatus

In this chapter, a description of the experimental facility used in the investigation is presented. The facility is designed for the study of the heat transfer coefficients and pressure drops of various refrigerants in various conditions. This apparatus has already been described in detail by Panek [1991], Christoffersen [1993], and Wattelet [1994] but, recently, some modifications have been made that have not been previously documented. Therefore, a brief description of the main features of the facility, as well as an account of the recent changes, is given.

3.1 Experimental Test Facility

The experimental facility is divided into four major systems: a refrigerant loop, a chiller system, a single-tube test section, and a data acquisition system. Subsequent sections in this chapter focus on each of these components and also describe the instrumentation used in the refrigerant loop and the test section.

3.1.1 Refrigerant Loop

Figure 3.1 shows a schematic of the refrigerant loop. Subcooled refrigerant is drawn from the condenser and circulated through the apparatus by a Micropump variable-speed gear pump. Use of this pump eliminates the need for a compressor and, since no oils are introduced into the system, pure refrigerants can be tested. Altering the speed of the gear pump is used to provide coarse control over the mass flux of the refrigerant flowing through the loop. A bypass line, which sends refrigerant back to the condenser, is utilized to give more precise control over the mass flux.

From the pump, the fluid flows through a Micro-Motion mass flow meter. Measurement of the mass flow rate of the fluid is described in more detail in section 3.2.1. The refrigerant then moves on to the preheater which consists of a three pass, horizontal, serpentine copper annulus with a 0.875 in. (22.2 mm) outside diameter and a 0.375 in. (9.53 mm) inside diameter. The 0.375 in. (9.53 mm) tube is secured inside the larger tube by means of a spirally wrapped wire. The reason for creating the annulus is that the system required a smaller charge of refrigerant with the preheater in this configuration then if the preheater was composed of the 0.875 in (22.2 mm) tube alone.

Heat to the preheater is provided by eleven Kapton electric resistance heaters wrapped around the outside of the annulus. These heaters supply approximately 500 W (1706 Btu/h) of power each and are controlled through four switches and a 115 Volt

Variac. Two of the switches furnish approximately 1500 W (5119 Btu/h) of power to the system, another inputs 1000 W (3412 Btu/h), and the remaining switch supplies 500 W (1706 Btu/h). The Variac is capable of providing a maximum power input of 1000 W (3412 Btu/h). This heat input is required to transform the refrigerant from a subcooled liquid into a two-phase fluid.

From the preheater, the two-phase refrigerant enters the test section by passing through the first of two sight glasses. These two sight glasses, the second of which is located at the exit of the test section, serve two purposes. The first is that they provide a means of determining the flow regime of the refrigerant entering and exiting the test section. They also allow visual confirmation of flow through the refrigeration loop. This ensures that no heaters are turned on without refrigerant flowing, as this might cause severe damage to the preheater and test section.

The test section, like the preheater, has electric resistance heaters wrapped around the outside of the tube. These heaters are used to provide a constant heat input into the refrigerant. From the temperatures and pressures measured in the test section, the heat transfer coefficient and the pressure drop of the fluid are calculated. Section 3.1.3 describes the test section more fully. After the test section, the two-phase refrigerant enters the condenser and is returned to the subcooled liquid state. The next section focuses on the condenser and the entire chiller system.

3.1.2 Chiller System

Heat is removed from the refrigerant via a counterflow, helical condenser that uses a 50/50 solution of ethylene glycol and water as its coolant. This type of condenser requires a charge between 2.7 and 5.9 kg (6 and 13 lbm), as compared to the approximately 9 kg (20 lbm) needed with a shell and tube heat exchanger. A slight disadvantage of the smaller condenser is that it can not act as a receiver, as some larger condensers do. Refrigerant must be periodically added or removed from the loop in order to maintain subcooling at the pump and preheater inlets.

Unlike the test refrigerant, the amount of ethylene glycol solution used in the chiller system remains constant. It is held in a 23 kg (50 lbm) storage tank. A thermocouple is used to monitor the temperature of the fluid in the tank. Through a chiller control panel, a set point is established. Two antifreeze pumps cycle on and off to maintain the tank temperature within ± 1.1 °C (± 2.0 °F) of the set point. The control panel not only regulates the tank temperature, it also controls the amount of heat removed. A hi-low setting on the chiller control panel selects which of two thermostatic expansion valves is used. One valve allows large amounts of heat removal at high temperatures and the other

removes less heat at lower temperatures. The heat acquired by the ethylene glycol loop is removed by an R-502 circuit that has a maximum heat removal rate of 17.5 kW (60,000 Btu/h). The R-502 loop then releases its heat into the municipal water supply.

When the amount of heat the chiller system is capable of removing equals the amount of heat the chiller absorbs, the refrigerant loop reaches a steady-state condition. Although the chiller system alone could be used to set the saturation temperature of the refrigerant loop, there is a drawback to this. The refrigerant loop would take a very long time to reach the desired temperature. Therefore, the saturation temperature of the refrigerant is established in the following manner. An artificially low set point is inputted into the chiller control panel. The chiller is then set to remove more heat than the refrigerant loop releases. A false load heater is used to supply the additional heat needed. Increasing or decreasing the heat provided by the false load heater raises or lowers the saturation temperature within the refrigerant loop. Figure 3.2 is a schematic of the chiller system.

3.1.3 Test Section

The test section consists of a 64 in. (1.63 m) long section of straight copper tubing. The copper tubing has an outer diameter of 0.375 in. (9.53 mm) and a wall thickness of 0.035 in. (0.89 mm). Four 57.3 Ohm Kapton electric resistance heaters with aluminum foil backing are wrapped longitudinally around the outside of the test section. The aluminum foil backing ensures that the heat input provided by the heaters is distributed uniformly.

In previous test sections, the heaters were not Kapton but silicon rubber. They were wrapped helically, not longitudinally, along the length of the tube. Sixteen thermocouples, placed at four different axial locations and four different circumferential locations were mounted in grooves on the test section surface. These thermocouples were used to measure the surface temperature of the tube. Figure 3.3 shows this thermocouple configuration. The thermocouples were carefully soldered to the tube, excess solder was removed to ensure a perfectly smooth surface, and high thermal conductivity epoxy was brushed on the solder bead to cover any exposed wire. Despite this care, extensive testing indicated that the surface temperatures were affected by the electric resistance heaters.

In order to avoid this unwanted influence, a new thermocouple configuration was designed. This design is shown in figure 3.4. In the new layout, Kapton heaters are wrapped longitudinally around the tube. Since the width of the heaters are not exactly equal to the circumference of the tube, part of the tube wall is left bare. The heaters are arranged so that these gaps occur at the top and bottom of the tube. Ten grooves, 0.02 in.

(0.5 mm) deep, are located within these gaps. In addition to these grooves, nine more are cut at three axial locations, 90° apart circumferentially.

Gauge 30, type T (copper-constantan) thermocouples are soldered in all the grooves. As in the previous test section, great care was taken in the mounting process. Unlike the gap thermocouples, the nine additional thermocouples fall underneath the strip heaters. Extensive single-phase testing was conducted with this test section and the experimental heat transfer coefficients were compared to those generated by various single-phase correlations. From these tests, it was determined that the surface temperatures measured by the gap thermocouples were artificially low. This is due to the absence of the heater covering. Surprisingly, the thermocouples under the heaters measured the correct temperature and were no longer influenced by the strip heaters. This change is attributed to the use of the longitudinal wrap as opposed to the spiral wrap and to the use of the different heater elements.

Along with the surface temperature, the bulk fluid temperatures are also measured. This is done in the adiabatic portion of the test section which is located before and after the heated length. Again, grooves are cut at the top and bottom of the tube and thirty gage thermocouples are carefully soldered into place. High thermal conductivity epoxy is used to cover any bare wires. As with the surface temperatures, extensive tests were conducted to check the validity of this method. Comparisons between this method of measuring the saturation temperature and using pressure transducers and saturated pressure-temperature curve fits showed an agreement of ±0.5 °F (±0.3 °C).

The pressure transducers are connected to the refrigerant loop by means of 0.125 in. (3.2 mm) o.d. copper tubing and pressure taps. These pressure taps are shown in figure 3.5. A tap is soldered to the tube at the desired location. A 0.06 in.(1.5 mm) hole is then drilled through the test section wall. The last step is to de-burr the hole using either a long cotton swab or a small piece of sandpaper. An absolute pressure transducer measures the pressure at the inlet of the test section while a differential pressure transducer is used to measure the test section pressure drop.

3.1.4 Data Acquisition System

The data acquisition system consists of the following components: a Macintosh II computer, four Strawberry Tree™ data acquisition boards, six Strawberry Tree™ terminal panels, and the data acquisition program called Analog Connection Workbench™. The data acquisition system performs a variety of tasks. It monitors and records output signals from the various temperature, pressure, and power transducers. It transforms these outputs, which are either 0-10 VDC or 4-20 mA signals depending on the device, into

quantities of interest, such as temperature or power. The data acquisition system program controls the false load heater by means of a 0-10 VDC analog output. Using curve fits and measured temperatures and pressures, it calculates important thermodynamic properties, such as the liquid enthalpy of the refrigerant entering the test section. All the information taken from the refrigerant loop is recorded at a sampling rate of one sample/second for a total of 60 seconds per test. This data, as well as several thermodynamic properties calculated by the program, are then transferred to the data reduction program. This program is described in further detail in section 4.2.

3.2 Instrumentation

This section focuses on the different measurement devices used in the experimental apparatus. These devices include flow meters, watt transducers, pressure transducers, and thermocouples.

3.2.1 Mass Flow Measurements

The mass flow rate of the fluid circulating through the refrigerant loop is measured with a Coriolis-type mass flow meter. This device, a D-12 Micro-Motion flow meter, has two small orifices located at both its inlet and outlet. The orifices help in dampening any oscillations that might be present in the flow.

A second flow meter is found in he chiller system. This flow meter, a Flow Technology turbine flow meter, measures the flow rate of the ethylene-glycol solution. This information is necessary in maintaining the set point temperature. Since the viscosity of the antifreeze solution is highly dependent on temperature, the flow meter had to be calibrated at three different viscosities to account for this effect.

3.2.2 Power Measurements

There are three Ohio Semitronics Watt transducers used in the refrigerant loop. One, model PC5-49D92, is used to measure the power that is generated by the test section heaters. Another, model PC5-50D292, is used to measure the heat rate inputted by the heaters controlled by the four preheater switches. The last transducer, model PC5-010D, measures the power input of the preheater contolled by the Variac. The uncertainty of all three devices is factory estimated at 0.2% of the full scale reading.

3.2.3 Pressure Measurements

Absolute pressure measurements are measured at three locations around the refrigerant loop. The first of these locations is at the preheater inlet. A BEC strain-gage

pressure transducer, with a range of 0-300 psia (0-2100 kPa), measures this pressure, which is used to determine the amount of preheater subcooling. In order for tests to be valid, the fluid entering the preheater must be a subcooled liquid. The second pressure transducer, which is the same model and has the same range as the above, measures the pressure at the inlet of the test section. This pressure transducer serves two purposes. It is used as a second check on the saturation temperature during two phase tests and, during single phase tests, it indicates the amount of subcooling available at the test section entrance. The last transducer is located at the entrance to the pump. This is a Sentra pressure transducer with a range of 0-6900 kPa (0-1000 psia). The pump inlet pressure is used to calculate the subcooling at the pump entrance. If there is insufficient subcooling, the pump does not operate at maximum efficiency. In addition to the absolute pressure transducers, a Sensotec differential pressure transducer with a range of 0-35 kPa (0-5 psi) measures the pressure drop across the test section. All four devices were periodically calibrated on a dead weight tester and have factory estimated uncertainties of ±0.3% of the full scale reading.

3.2.4 Temperature Measurements

All thermocouples used in the system have been calibrated using a Neslab constant temperature bath and NIST traceable, high precision thermometers. Instead of the integral cold junction sensor built into the data acquisition terminal panels, an ice bath is used as the reference state and voltage differences are used in the calibration curves. This method was adopted because, with the cold junction, the measured surface temperatures proved to vary greatly with position on the terminal panel. The thermocouples are calibrated over a range of 18 to 104 °F (-8 to 40 °C), with a different calibration for every thermocouple terminal panel. The uncertainty of the temperature measurements is estimated to be ±0.36 °F(±0.2°C).

There are two methods used to measure the temperature throughout the refrigerant loop and test section. The first, mentioned in section 3.1.3, utilizes thermocouples soldered in grooves cut into the surface of the test section. In the second method, thermocouples protected by a stainless steel sheath extend directly into the refrigerant flow. The three probes of interest are placed in the following locations: before the pump, before the preheater, and before the test section. The probe at the pump inlet is used to calculate the pump subcooling, the one before the preheater is used to calculate the preheater subcooling as well as the refrigerant's liquid enthalpy, and the probe before the test section is a redundant check on the saturation temperature.

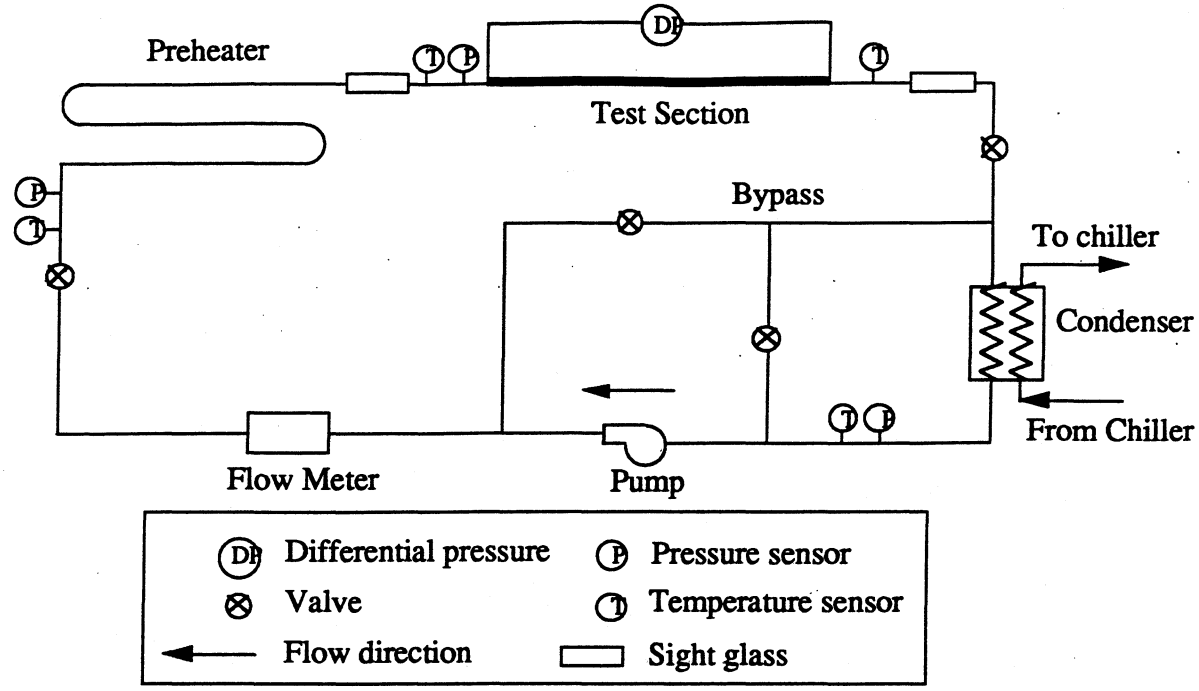

Figure 3.1 Experimental apparatus

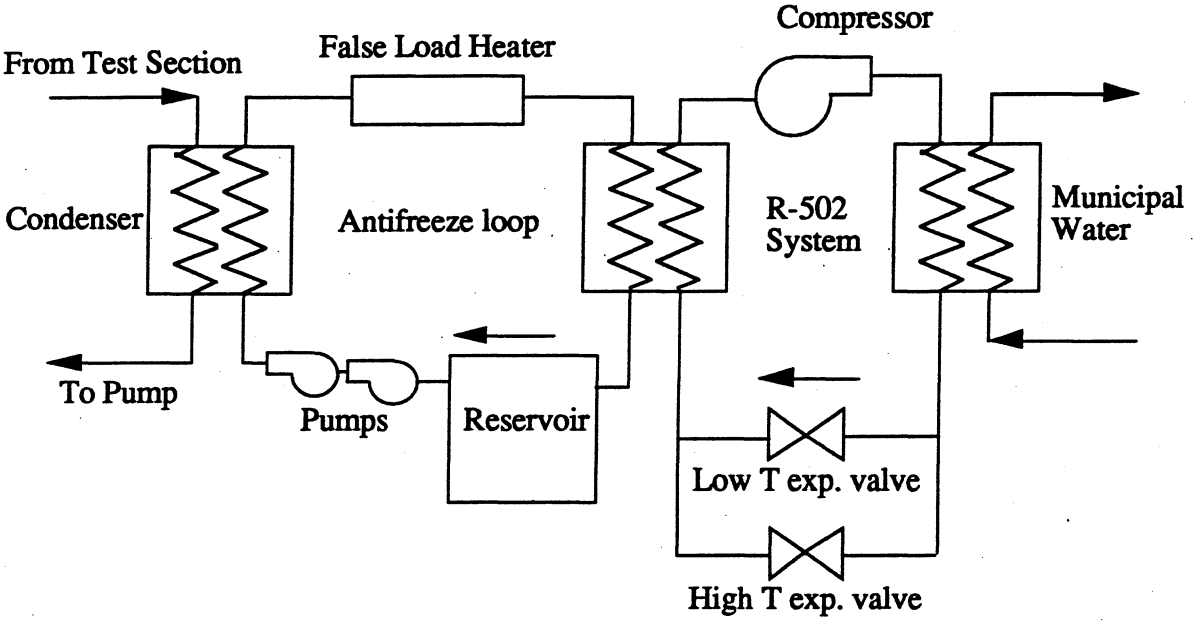

Figure 3.2 Schematic of chiller system

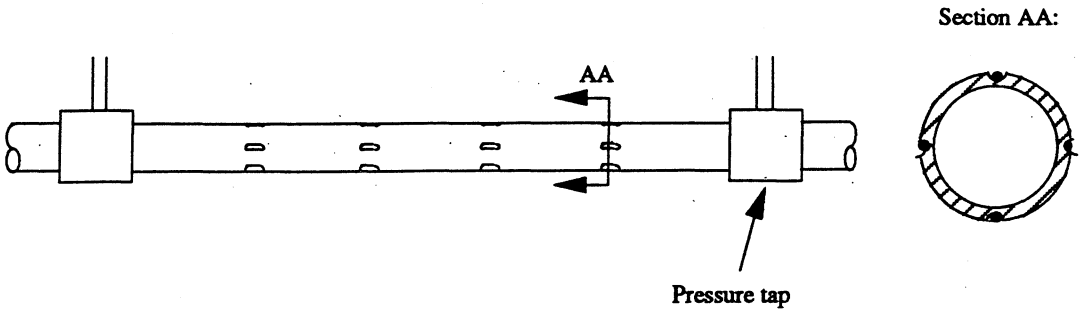

Figure 3.3 Schematic of previous test section

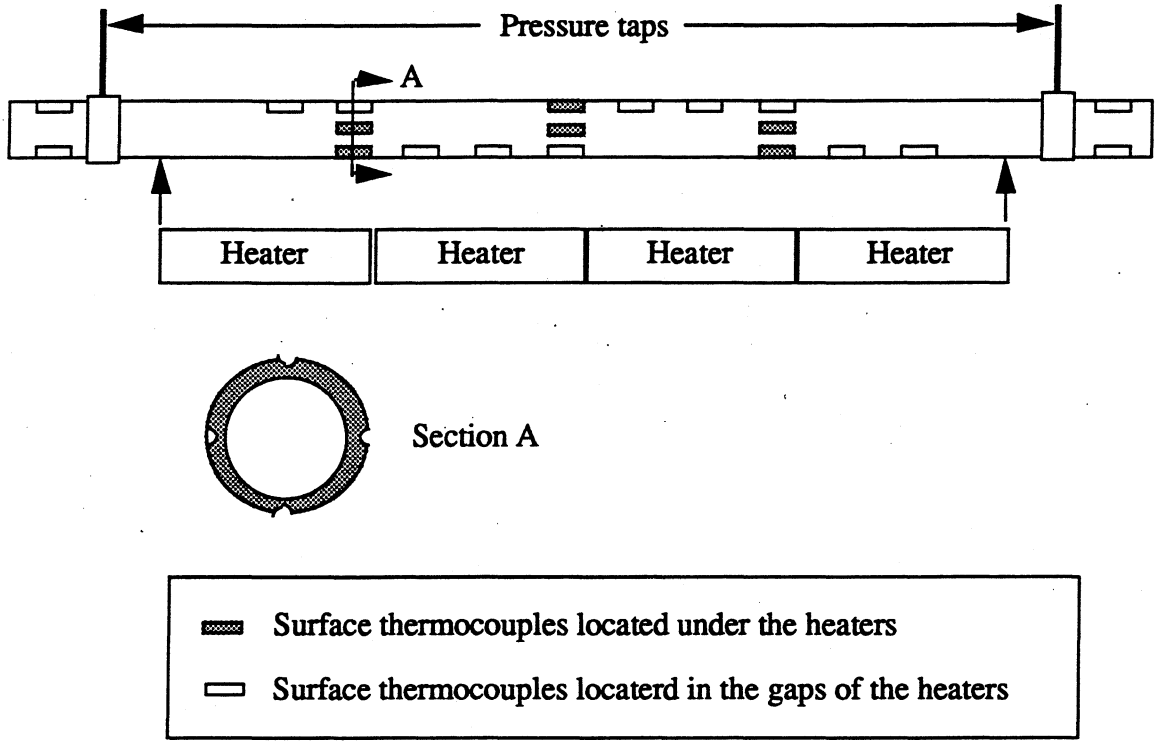

Figure 3.4 Schematic of the new test section

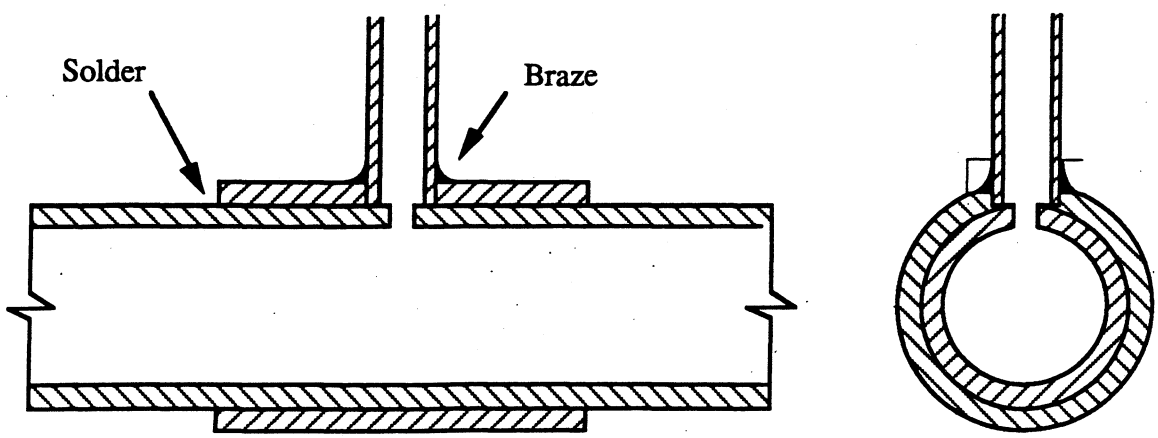

Figure 3.5 Pressure tap.

CHAPTER 4
Experimental Procedures

For each new set of experiments, a series of steps must be followed to ensure the validity of the experimental data collected. This chapter outlines the preparation of the experimental apparatus and the procedures used to gather the data. This account is followed by an explanation of how the single phase and two phase heat transfer coefficients, as well as heat gains and experimental uncertainties, are calculated. Validation testing, which confirms that all the systems are functioning normally, is also discussed. Finally, the range of conditions over which the data is collected is presented.

4.1 Experimental Facility Operation

This section is divided into two parts. The first part describes the procedures that must be followed prior to running a new set of tests. These steps are performed only once and are repeated only if the test refrigerant or the test section is changed. The next section details the regular operation of the experimental apparatus.

4.1.1 System Preparation

Before testing with a new refrigerant or after the installation of a new test section, the entire refrigerant loop is evacuated to remove any contaminants, such as air or old refrigerant. The loop is kept under vacuum and two ball valves, which divide the apparatus into two sections, are closed. Thus, if any leaks are present, their exact location can be more easily determined. If the pressure in both sections increases significantly over a period of time, there is a leak in both sections. However, if only one section experiences a pressure increase, only that section must be examined. Once it has been established that there is a leak, compression fittings are tightened and Teflon tape is re-applied to the fittings.

The vacuum test is limited in that it can only indicate the presence of a leak but not its exact location. The exact location of the leak is ascertained in the following manner. The ball valves are opened and the loop is charged with vapor R-134a to a pressure of about 500 kPa (72 psia). Again, the loop is divided into two sections. The pressure in both sections is monitored. Rapidly decreasing pressure in one or both sections indicates the presence of a leak. Both a soapy water solution and an electronic leak detector are used to check all joints, fittings, and connections. These are tightened, re soldered, or replaced as is necessary. The loop is then allowed to sit overnight. If the pressure remains constant, with fluctuations due to temperature variations taken into consideration, the loop

is assumed to be free of leaks. The refrigerant loop is again evacuated and then filled with the test refrigerant.

4.1.2 Data Collection Procedures

Before starting up the system, certain checks are made to guarantee that all the parts of the equipment are working properly. After the data acquisition computer is turned on, the ice bath is filled with a fresh mixture of crushed ice and water and the temperatures and pressures are inspected to make certain they fall within normal bounds. Then the refrigerant pump is turned on. Once flow is established, the chiller pumps are started up and the set point is inputted into the chiller control panel. The next step is to supply power to the preheater and test section heaters. The equipment is now operational and specific test conditions can be set.

The parameters varied during the experiments are as follows: mass flux, inlet quality, heat flux, and saturation temperature. First, the mass flux is adjusted by means of the variable-speed gear pump controller and the bypass line. When the mass flux reaches the desired value, the inlet quality set is by using an appropriate combination of preheater switches and the Variac setting. Changing the inlet quality affects the mass flux, especially at low flow rates, so both must be continually adjusted. The test section heat flux is then set. The last parameter fixed is the saturation temperature. Since this is influenced by both the inlet quality and the test section heat flux, all other variables must be set before any changes to the temperature can be made. The saturation temperature is controlled by setting the false load heater output and the set point temperature.

Once all of the conditions are set, the refrigerant loop is allowed to reach steady state before a test can be recorded. This time required to reach this point varies from as little as 15 minutes to as long as several hours. Steady state is reached when the variables of interest remain within the following range of target values for several minutes: saturation temperature, ± 0.2 °C (± 0.36 °F); mass flux, ± 5%; heat flux, ± 5%. When this occurs, the data is logged into a data acquisition output file for one minute. The output is then transferred to a data reduction program which is used to calculate the heat transfer coefficients.

4.2 Data Reduction

The data reduction program consists of three Microsoft Excel spreadsheets. The first spreadsheet contains the test section dimensions and the thermophysical property curve fits for the test refrigerant. These curve fits, which include saturation pressure as a function of temperature, were generated from data provided by Dupont. The test

refrigerant used in this study, R32/R125 (45/55 %), is a near azeotrope which exhibits a small difference in saturation pressure between the liquid and vapor components at the same temperatures. For example, at 41 °F (5 °C), the vapor saturation pressure is 134 psia (923 kPa) while the liquid saturation pressure is 134.6 psia (928 kPa). This difference is very small and falls with the uncertainty of the pressure transducers, so the saturation pressure used is an average of the liquid and vapor pressures. Appendix A contains the curves fits used in this study.

The property spreadsheet is linked to a second spreadsheet which uses this information to perform a variety of functions. The second spreadsheet averages the raw data collected by the data acquisition program. It uses this data in combination with the thermophysical properties to calculate the experimental heat transfer coefficients. Additionally, it also computes the heat transfer coefficients predicted by several two-phase correlations. The final spreadsheet lays all this information out in a clear and concise format.

The data of chief importance in this study are the experimental heat transfer coefficients and pressure drops. Although the pressure drop through the tube can be directly measured by means of the differential pressure transducer, the heat transfer coefficient, h, can not and must be calculated. The equation used in these calculations is Newton's law of cooling which is defined as:

$$h = \frac{q/A_s}{\left(\overline{T}_s - \overline{T}_b\right)} \tag{4.1}$$

The variable A_S represents the inside surface area of the heated section. This is the area directly covered by the test section strip heaters. The average surface temperature of the tube is represented by T_S. This is measured by the thermocouples soldered into grooves on the outside of the test section. Only the thermocouples covered by the strip heaters are used in the calculation. Although the quantity of interest is the inside wall temperature, calculations by Wattelet [1994] show that the temperature drop across the wall is negligible and can be ignored. The bulk fluid temperature, T_b, is a value that is derived from linearly interpolating the average inlet and outlet temperatures measured in the adiabatic portion of the test section. Finally, q is the heat input rate into the test section.

The amount of heat delivered by the test section strip heaters should equal the amount of heat absorbed by the refrigerant in the test section. However, single phase energy balances indicate that there is a slight discrepancy between these values. Energy balance testing conducted over a wide range of test conditions show that the heat gain

experienced by the test section is approximately 5 W (17 Btu/h). This correction was added to the data acquisition program. There is also a similar discrepancy present in the preheater energy balances. This heat gain from the environment was found to be on the order of 10 W (34 Btu/h). Again, a correction was included in the data acquisition program. Although the differences in the heat supplied by the heaters and the actual heat absorbed by the test refrigerant is not great, these differences could slightly affect certain important parameters, such as inlet quality.

The inlet quality is calculated though an energy balance performed over the preheater. The fluid at the entrance of the preheater is a subcooled liquid. Its enthalpy is assumed to be approximately equal to the enthalpy of saturated liquid at the same temperature. As discussed by Wattelet [1994], this approximation results in a negligible error. The enthalpy of the refrigerant exiting the preheater is defined in the following equations:

$$i_{preheater,out} = \frac{q_{preheater}}{\dot{m}} + i_{preheater,in} \tag{4.2}$$

where

$$i_{preheater,in} = i_l\left(T_{preheater,in}\right) \tag{4.3}$$

In the preceding equations, i is the enthalpy of the refrigerant at a specific location, i_l is the saturated liquid enthalpy as a function of refrigerant temperature, and $\dot{m}$ is the mass flow rate of the refrigerant. Since the preheater ends where the test section begins, the enthalpy of the fluid exiting the preheater equals the enthalpy of the fluid entering the test section. Using this information and the enthalpy of vaporization, i_{lv}, calculated at the test section inlet temperature, the inlet quality is determined in the following manner:

$$x_i = \frac{i_{preheater,out} - i_l\left(T_{testsection,in}\right)}{i_{lv}\left(T_{testsection,in}\right)} \tag{4.4}$$

The test section outlet quality is calculated in a similar fashion to the inlet quality. As in the preheater, an energy balance is performed and the following expression for outlet quality, x_o, is derived:

$$x_o = \frac{i_{testsection,out} - i_l\left(T_{testsection,out}\right)}{i_{lv}\left(T_{testsection,out}\right)} \tag{4.5}$$

where

$$i_{test\,section,out} = \frac{q_{test\,section}}{\dot{m}} + i_{test\,section,in} \tag{4.6}$$

4.3 Data Validation

The experimental apparatus contains several redundant checks on the various instruments used during testing. The accuracy of the bulk temperature thermocouples in measuring the saturation temperature is verified by comparing that temperature to the temperature calculated using the pressure and the saturated temperature-pressure curve fits. These temperatures are within ± 0.36 °F (0.2 °C) of each other. Along with the bulk fluid temperatures, the watt transducers were also checked to ensure they were operating properly. The voltage across the preheater and test sections heaters was measured with a multimeter. Using this information and the resistance of the heaters, the power supplied was calculated. This value agreed within 10 W (34 Btu/h) of the watt transducer reading.

The surface thermocouples were checked by means of single phase energy balance testing. These single phase tests were performed with both R134a and the R32/R125 mixture. The experimental heat transfer correlations derived from these tests were compared to those predicted by the Dittus-Boelter [1930], Petukhov [1970], and the Gnielinski [1976] correlations. For the entire range of single phase tests, the experimental values fell within ± 10% of the Dittus-Boelter and Gnielinski correlations. The Petukhov correlation did not perform as well as the others. The experimental values fell within ±12% of its predictions. This is shown in Figure 4.1. Table 4.1 shows the mean deviation of the three correlations compared with the experimental data.

Table 4.1 Mean deviation of single phase correlations

CORRELATION	MEAN DEVIATION	
	R134a	R32/R125
Dittus-Boelter	1.7%	2.2%
Petukov	9.4%	8.2%
Gnielinski	5.3%	6.7%

4.4 Uncertainty Analysis

The experimental uncertainty is calculated using the method of sequential perturbation as described by Moffat [1988]. First, a base heat transfer coefficient is calculated from experimental data. Then, each independent variable used to calculate the

heat transfer coefficient is perturbed by its uncertainty and a new heat transfer coefficient is determined. Table 4.2 contains the uncertainty of each input. Once all the heat transfer coefficients are calculated, the square root of their sums is taken. The difference between this value and the base case is the maximum error. Equation 4.7 summarizes this method and the uncertainties are listed in Appendix B.

$$\partial h = \left[\left(\frac{\partial h}{\partial \dot{Q}_{TS}} \partial \dot{Q}_{TS} \right)^2 + \left(\frac{\partial h}{\partial d_i} \partial d_i \right)^2 + \left(\frac{\partial h}{\partial L_{HX}} \partial L_{HX} \right)^2 + \left(\frac{\partial h}{\partial \overline{T}_s} \partial \overline{T}_s \right)^2 + \left(\frac{\partial h}{\partial \overline{T}_b} \partial \overline{T}_b \right)^2 \right]^{1/2} \quad (4.7)$$

Table 4.2 Parameter uncertainties

Parameters	Uncertainties
Inside diameter, d_i	± 0.003 in. (0.08 mm)
Heated length, L_{HX}	± 0.125 in. (3.2 mm)
Surface temperature, $\overline{T}_s$	0.36 °F (0.2 °C)
Bulk fluid temperature, $\overline{T}_b$	0.36 °F (0.2 °C)
Test section heat input, $\dot{Q}_{TS}$	34 Btu/h (10 W)

4.5 Test Matrix

The conditions in which the experiments were conducted are listed in table 4.3. The variable ranges were chosen to simulate the conditions typically found in a stationary air-conditioning and medium-size refrigeration system.

Table 4.3 Test Conditions

Parameter	Conditions
Inlet saturation temperature	41°F (5 °C)
Mass flux	37-370 $\frac{klb_m}{ft^2 \cdot hr}$ (50-500 $\frac{kg}{m^2 \cdot s}$)
Inlet quality	20-80%
Test section heat flux	640-9500 $\frac{Btu}{h \cdot ft^2}$ (2-30 $\frac{kW}{m^2}$)

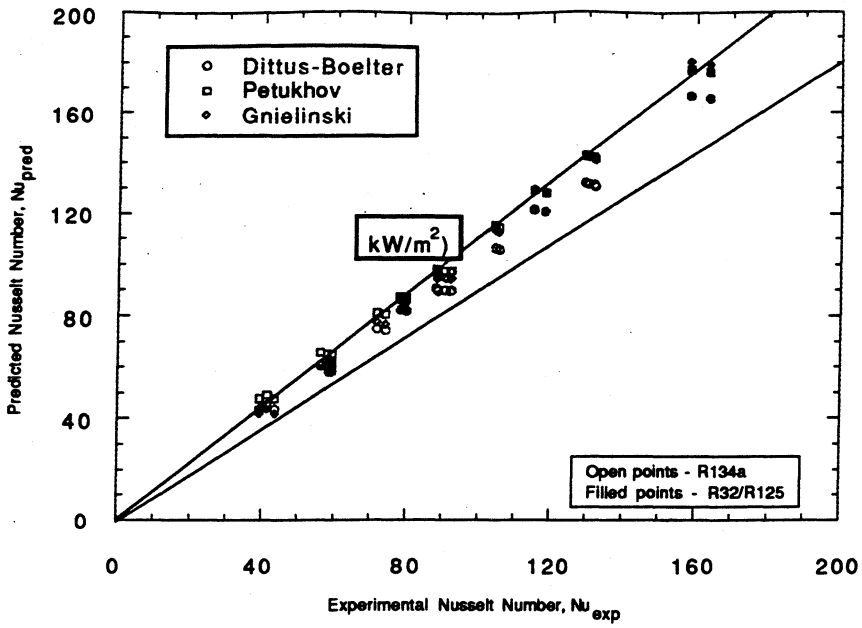

Figure 4.1 Experimental single-phase Nusselt number versus predicted single-phase Nusselt number

CHAPTER 5
Experimental Results

In this chapter, the experimental results are examined. The effect of mass flux, heat flux, and quality on the data is analyzed. The data are compared to several correlations used to predict the two-phase heat transfer coefficient and the pressure drop. Additionally, the heat transfer data is compared to other R32/R125 mixture results. All the data from the study are contained in Appendix B.

5.1 Heat Transfer Results

All the heat transfer data presented in this section are given in terms of Nusselt number, Nu, instead of heat transfer coefficients. Since Nusselt number is a dimensionless form of the heat transfer coefficient, this approach allows the units to be disregarded. The section begins with an examination of the behavior of the Nusselt number with respect to mass flux, heat flux, and quality. This is followed by a comparison of this data to that gathered by Christoffersen [1993]. The refrigerant in the Christoffersen study has a slightly different composition than the present one. Finally, the accuracy of several correlations in predicting the experimental results is compared.

5.1.1 Effects of Mass Flux, Heat Flux, and Quality

Figure 5.1 shows how the experimental Nusselt number, at a mass flux of 370 x 10^3 lb_m/ft^2-h (500 kg/m^2-s), varies with quality and heat flux. At low heat fluxes, 1600-3200 Btu/ft^2-h (5-10 kW/m^2), the Nusselt number is highly dependent on the quality, increasing as the quality increases. At the higher heat fluxes, the Nusselt number increases only slightly with quality. At an average quality of 60%, there is no longer any dependence on heat flux. These trends also occur at a mass flux of 220 x 10^3 lb_m/ft^2-h (300 kg/m^2-s). This is shown in figure 5.2. Above a quality of 80%, there is no heat flux dependence. At low heat fluxes, the Nusselt number is influenced more by quality than at higher heat fluxes. At heat fluxes above 3200 Btu/ft^2-h (10 kW/m^2) the Nusselt number exhibits no dependence on quality. Similarly, at a mass flux of 150 x 10^3 lb_m/ft^2-h (200 kg/m^2-s), the dependence on quality is more pronounced at the lower heat fluxes. This trend is shown in figure 5.3. At a heat flux of 6400 Btu/ft^2-h (20 kW/m^2), there is a slight decrease in the Nusselt number but this decrease falls within the experimental uncertainty.

For all of the conditions described above, the flow regime was usually observed to be annular. In annular flow, the dominant mode of heat transfer is convective boiling; however, nucleate boiling can be important at low qualities and high heat fluxes. As

explained in section 2.2, convective boiling is a function of quality and mass flux while nucleate boiling is dependent on the heat flux. At low heat fluxes and low qualities, the Nusselt number is influenced by both the quality and the heat flux. Thus, both mechanisms of heat transfer are present. As the quality increases, nucleate boiling is suppressed and convective heat transfer dominates. For a mass flux of 370 x 10^3 lb_m/ft^2-h (500 kg/m^2-s), this suppression takes place at a quality of 60%, while at a mass flux of 220 x 10^3 lb_m/ft^2-h (300 kg/m^2-s), the suppression occurs at a quality of 80%. At very high heat fluxes, where the Nusselt number shows no quality dependence, heat transfer is due mainly to nucleate boiling.

At mass fluxes of 75 x 10^3 lb_m/ft^2-h (100 kg/m^2-s) and 37 x 10^3 lb_m/ft^2-h (50 kg/m^2-s), the Nusselt numbers don't exhibit any significant quality dependence. The Nusselt number only increases with increasing heat flux. This is shown in figures 5.4 and 5.5. For a mass flux of 75x 10^3 lb_m/ft^2-h (100 kg/m^2-s) and a heat flux of 1600 Btu/ft^2-h (5 kW/m^2), there is a large drop in the Nusselt number at a quality above 80%. This decline is attributed to dry out of the flow. All the liquid evaporates and only vapor or mist flows through the tube. Since the thermal conductivity of vapor is much less than that of liquid, the Nusselt number is decreased. This is also seen in figure 5.5 at a quality of approximately 87%. For mass fluxes of 75 x 10^3 lb_m/ft^2-h (100 kg/m^2-s) and 37 x 10^3 lb_m/ft^2-h (50 kg/m^2-s), the refrigerant is primarily in the wavy or stratified regimes. In these regimes, nucleate boiling is dominant. This can be seen in the dependence on the heat flux and the lack of influence of the quality.

5.1.2 Comparison with Previous Studies

Many studies have been conducted that use refrigerant mixtures as the test fluid. Unfortunately, most of these studies differ sufficiently from the present one as to make any comparison impossible. Some investigators used different refrigerant mixtures. Others isolated the nucleate and convective boiling components of evaporative heat transfer [Jung et al., 1989]. Many have focused on the effects of mixtures in pool boiling.

Christoffersen [1993] tested a mixture of R32/R125 in a tube with a 0.375 in. (9.53 mm) o.d. The composition of this mixture was 60/40 % by weight, not the 45/55 % by weight used in the present study. The 60/40 mixture is closer to the azeotropic point, as show by the very small difference between the saturation pressure of the liquid and the vapor at a given temperature. For example, at 41°F (5 °C), the difference in saturated pressure for the

60/40 mixture is 0.14 psia (1 kPa). For the 45/55 mixture at the same temperature, the difference is 0.6 psia (5 kPa). The difference in their glides is very small and there should be very little difference between the experimental Nusselt numbers.

Figures 5.6 through 5.8 show that for the same mass flux, heat flux, and approximately the same quality, there is good agreement between the present data and the Christoffersen data. For all mass fluxes, the 60/40 mixture data show a dependence on quality at low heat fluxes but no dependence at high heat fluxes. This is the same behavior displayed by the 45/55 mixture. No comparisons can be made at the lower mass fluxes since Christoffersen did not take any data below a mass flux of 150 x 10^3 lb_m/ft^2-h (200 kg/m^2-s).

5.1.3 Comparisons with Correlations

In order to calculate the predicted Nusselt number, property data for the refrigerant are needed. The various properties are calculated through two different means. The first is to curve fit mixture property data provided by DuPont. The second method uses ideal mixture rules outlined in Kedzierski [1992], to combine the properties of pure R32 and pure R125. Kedzierski [1992] states that the mixing rule used to calculate the mixture properties can affect the results and it is important to state which mixing rule is used. A comparison between the predicted values using the ideal mixing rule properties and the curve fit properties was performed and is discussed in further detail below.

Figures 5.9 and 5.10 show the experimental Nusselt number versus the Nusselt number predicted by Shah's [1976] correlation. Although the Shah correlation was developed for pure fluids, the mixture is very nearly an azeotrope and pure correlations should predict its behavior well. As can be seen from the graphs, the Shah correlation tends to underpredict the data. A large portion of the points fall between the -20% and -40% lines. The Shah correlation also underpredicted the data gathered by Jung et al. [1989]. Jung attributed this to an underestimation of the convective contribution. Since Shah used a "greater of two' method, the convective contribution becomes the total heat transfer coefficient for many flow conditions. This reasoning explains why the present data is underpredicted. For figure 5.10, the ideal mixing rule was used to calculate the refrigerant properties. The accuracy of the predicted results decreased slightly.

In figures 5.11 and 5.12, the experimental Nusselt number is compared to the Jung and Radermacher [1989] correlation. This correlation tends to overpredict the heat transfer coefficient. Using the ideal mixing law properties causes the predicted Nusselt number to increase slightly. The reason for this lack of agreement is attributed to the surface tension used in the correlation. Since surface tension experimental data which is specific to

R32/R125 is hard to find, it was calculated using Brock and Bird's [1955] predictive method. This correlation might not accurately describe the mixture behavior.

The final correlation used is the Wattelet [1994] correlation. As can be seen from figures 5.13 and 5.14, the values predicted by this correlation have the best agreement with the experimental values. Using mixture properties based on the DuPont property data, all the points fall well within ± 20%. A majority of the points are within ± 10%. The agreement between the experimental and predicted Nu is not as close when the mixture properties are calculated with the ideal mixing rules. The predicted values are increased significantly and most of the values fall within +20% and +40%. This shows that the Wattelet correlation is more sensitive to the refrigerant properties than either of the others.

5.2 Pressure Drop Results

Figures 5.15 through 5.19 show that as the mass flux increases, the pressure drop also increases. These figures also show that, for all mass fluxes, the pressure drop exhibits a dependence on quality and heat flux. As both of those parameters are increased, the pressure drop increases. At mass fluxes of 75 x 10^3 lb_m/ft^2-h (100 kg/m^2-s) or less, this effect is very small and is not easily seen on the graphs. The effect of these variables increases as the mass flux increases with the most pronounced effect occurring at a mass flux of 370 x 10^3 lb_m/ft^2-h (500 kg/m^2-s).

The pressure drop is divided into two components, the frictional pressure drop and the acceleration pressure drop. Both the frictional pressure drop and the acceleration pressure drop are functions of mass flux. Increasing the mass flux increases both components. Additionally, the frictional pressure drop increases as the vapor velocity increases; thus, as the quality is increased, so is the pressure drop. The acceleration pressure drop is a function of the inlet and outlet qualities. The value for the outlet quality is affected by the amount of heat added to the system. The more heat added, the higher the outlet quality. Increasing the heat flux increases the acceleration pressure drop component.

The trends described above also describe the pressure drop data gathered by Christoffersen [1992]. Figures 5.20-5.22 show that the agreement between the two sets of data is very good for all conditions. Any differences between the results fall well within the experimental uncertainty.

Finally, figure 5.23 shows the experimental pressure drop plotted versus the pressure drop predicted by the Sousa [1993] correlation. All the points fall within ± 10%. This shows that the correlation can accurately predict the pressure drop behavior of the refrigerant mixture.

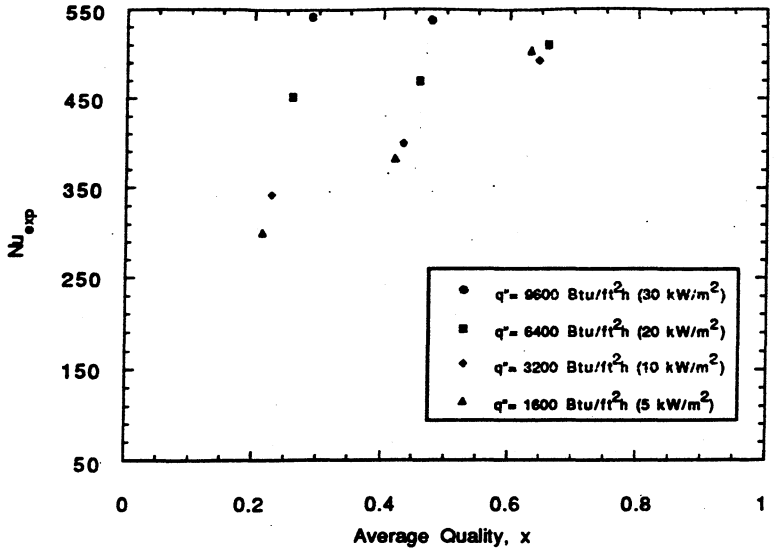

Figure 5.1 Experimental Nusselt number versus average quality at G=370 x 10^3 Btu/ft^2-h (500 kg/m^2-s)

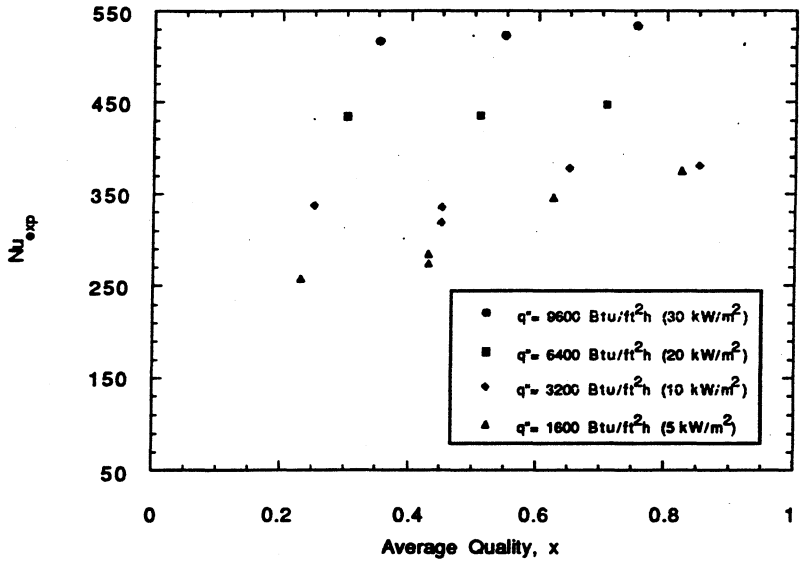

Figure 5.2 Experimental Nusselt number versus average quality at G=220 x 10^3 Btu/ft^2-h (300 kg/m^2-s)

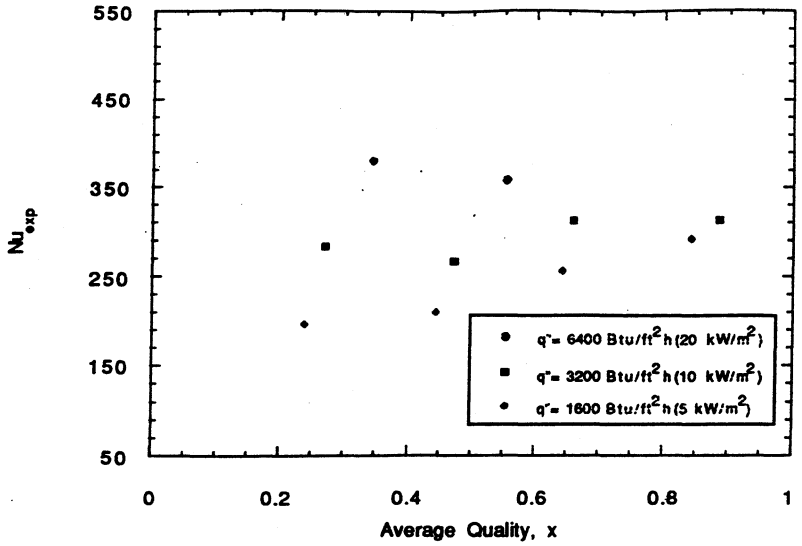

Figure 5.3 Experimental Nusselt number versus average quality at G=150 x 10^3 Btu/ft^2-h (200 kg/m^2-s)

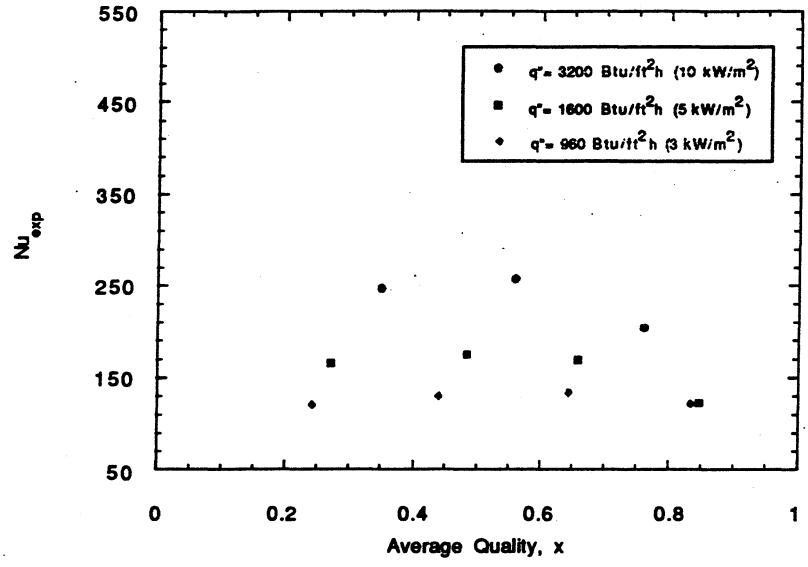

Figure 5.4 Experimental Nusselt number versus average quality at G=75 x 10^3 Btu/ft^2-h (100 kg/m^2-s)

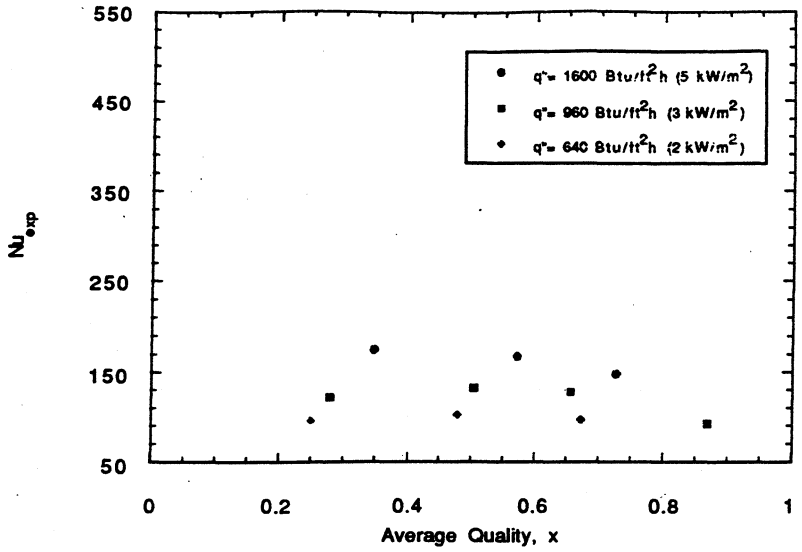

Figure 5.5 Experimental Nusselt number versus average quality at G=37 x 10^3 Btu/ft^2-h (50 kg/m^2-s)

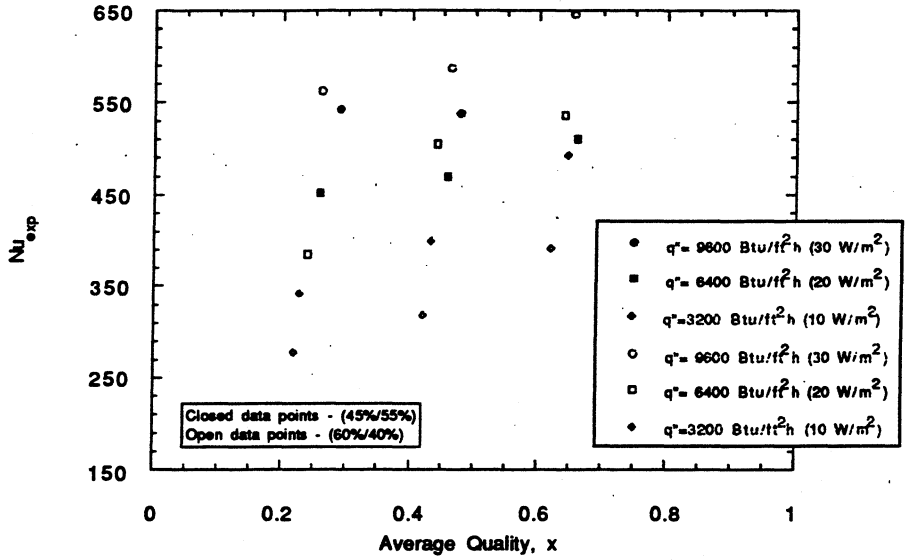

Figure 5.6 Comparison of experimental Nusselt numbers to Christoffersen's [1993] Nusselt numbers at G=370 x 10^3 Btu/ft^2-h (500 kg/m^2-s)

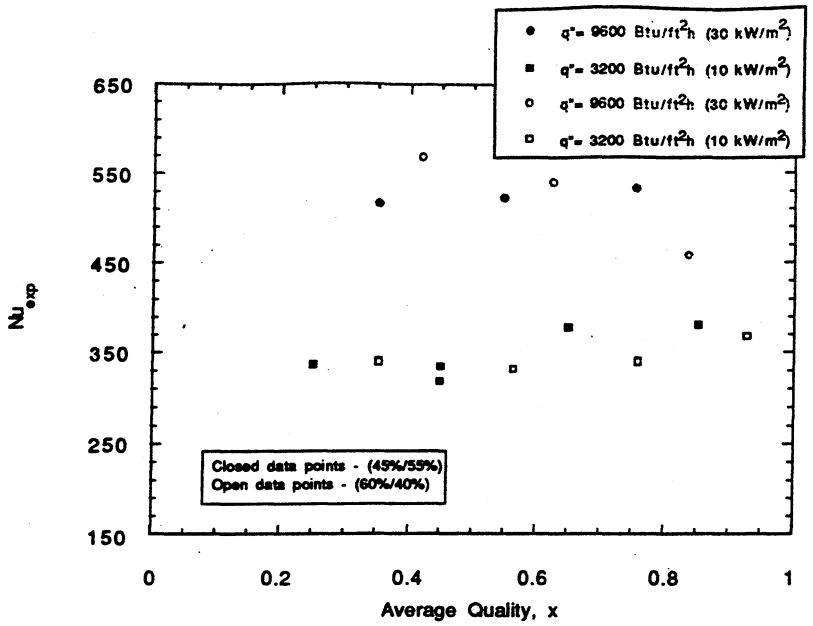

Figure 5.7 Comparison of experimental Nusselt numbers to Christoffersen's [1993] Nusselt numbers at G=220 x 10^3 Btu/ft^2-h (300 kg/m^2-s)

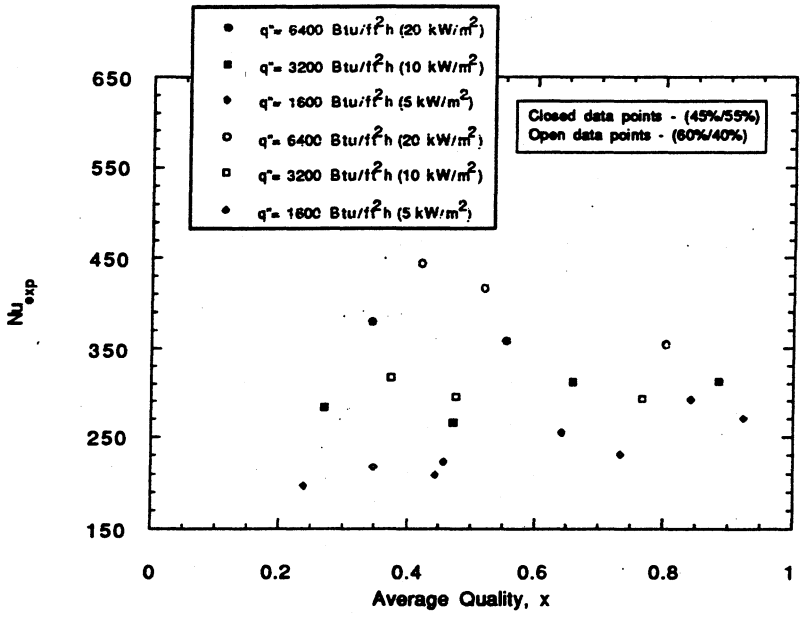

Figure 5.8 Comparison of experimental Nusselt numbers to Christoffersen's [1993] Nusselt numbers at G=150 x 10^3 Btu/ft^2-h (200 kg/m^2-s)

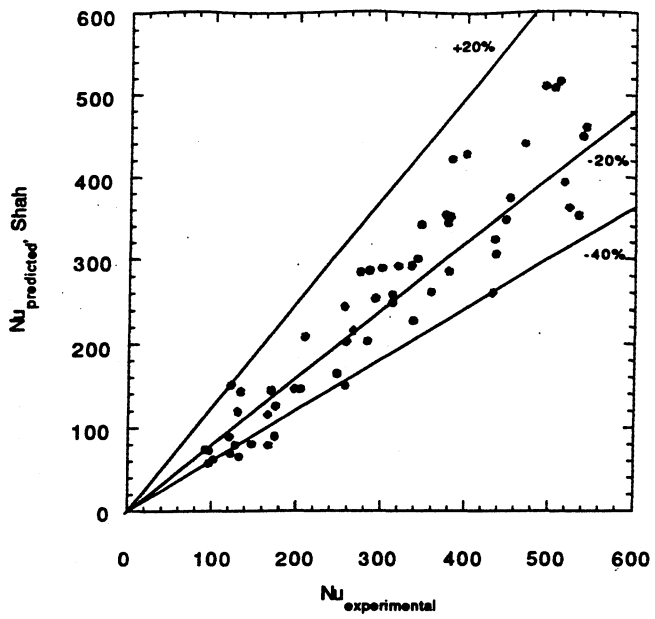

Figure 5.9 Experimental Nusselt number versus predicted Nusselt number for Shah correlation (DuPont property data)

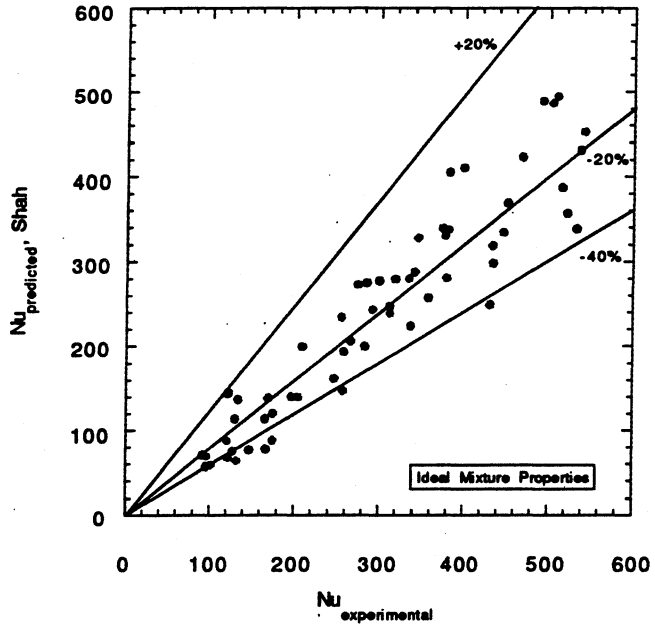

Figure 5.10 Experimental Nusselt number versus predicted Nusselt number for Shah correlation (Ideal mixture properties)

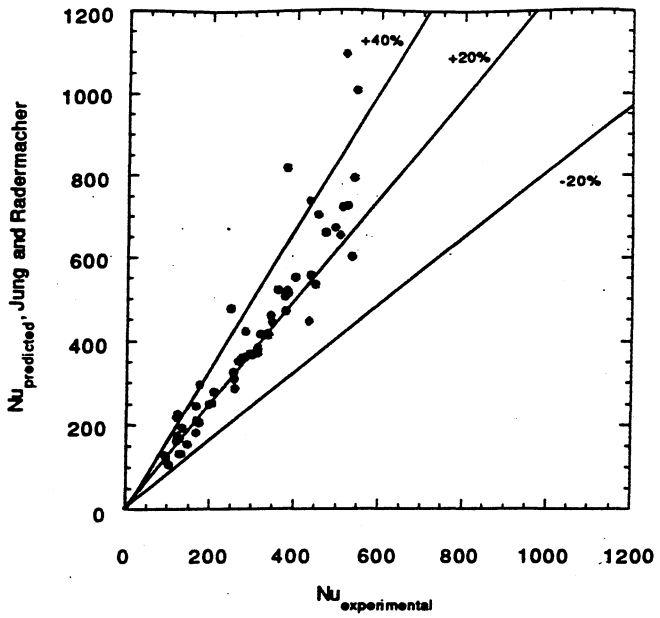

Figure 5.11 Experimental Nusselt number versus predicted Nusselt number for Jung and Radermacher correlation (DuPont property data)

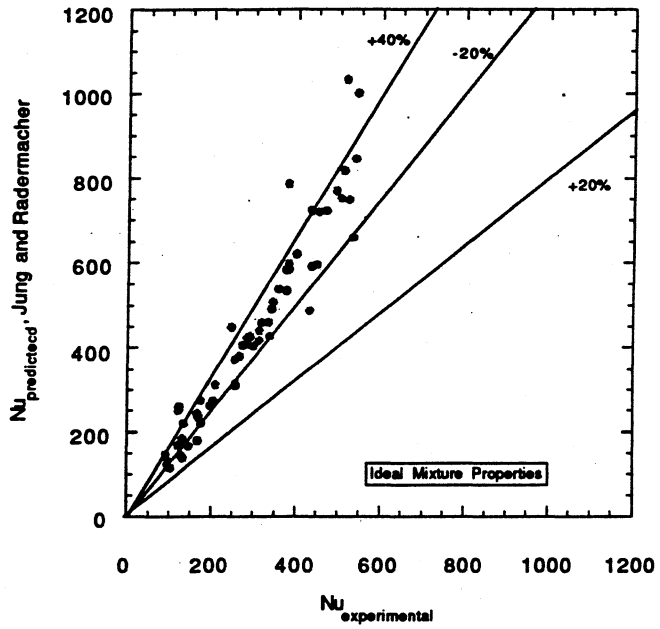

Figure 5.12 Experimental Nusselt number versus predicted Nusselt number for Jung and Radermacher correlation (Ideal mixture properties)

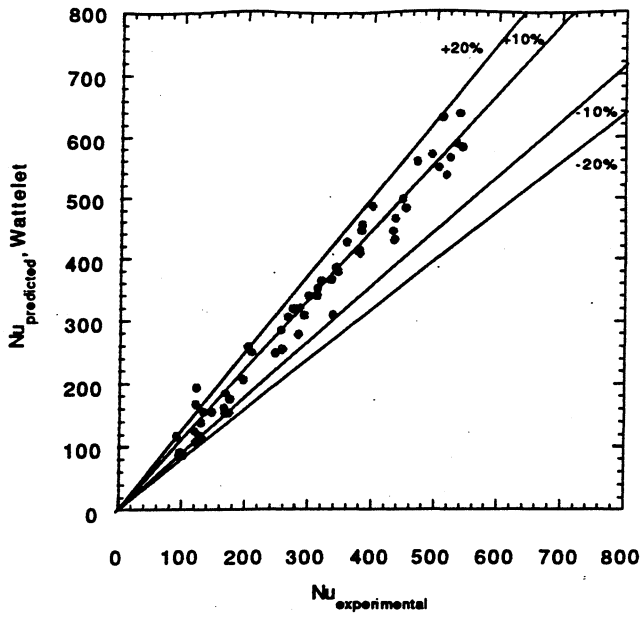

Figure 5.13 Experimental Nusselt number versus predicted Nusselt number for Wattelet correlation (DuPont property data)

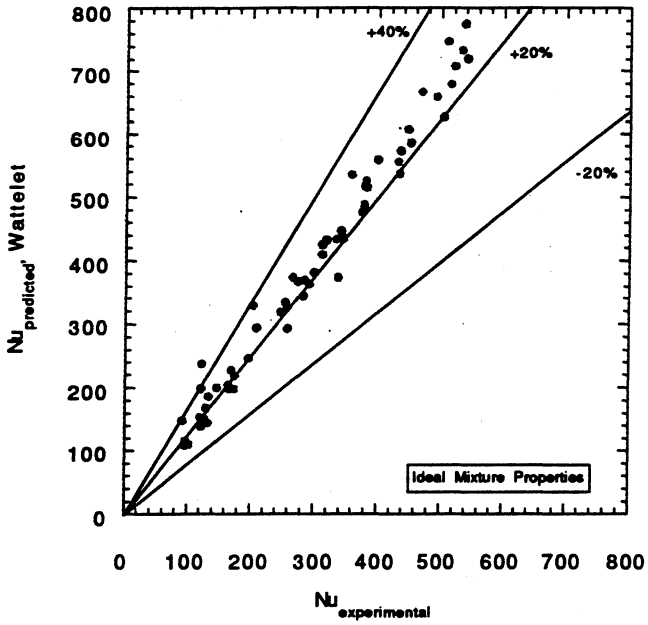

Figure 5.14 Experimental Nusselt number versus predicted Nusselt number for Wattelet correlation (Ideal mixture properties)

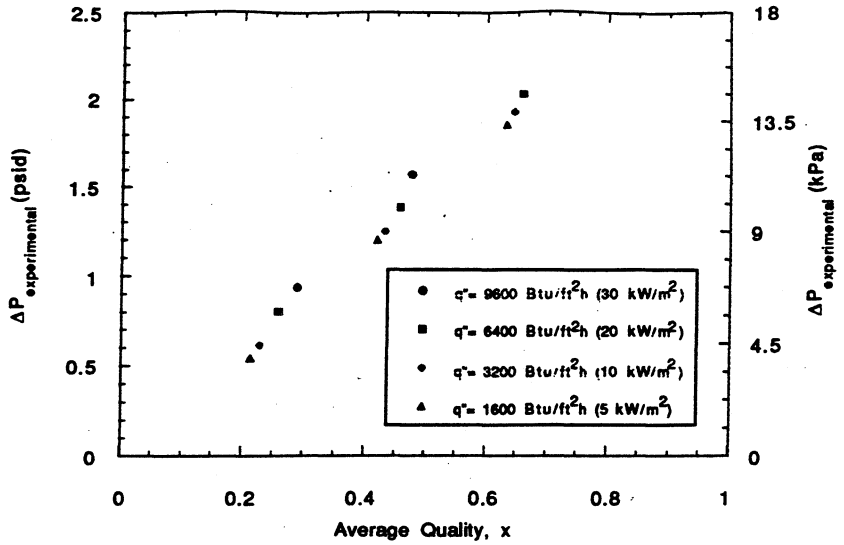

Figure 5.15 Experimental pressure drop versus average quality at G=370 x 10^3 Btu/ft^2-h (500 kg/m^2-s)

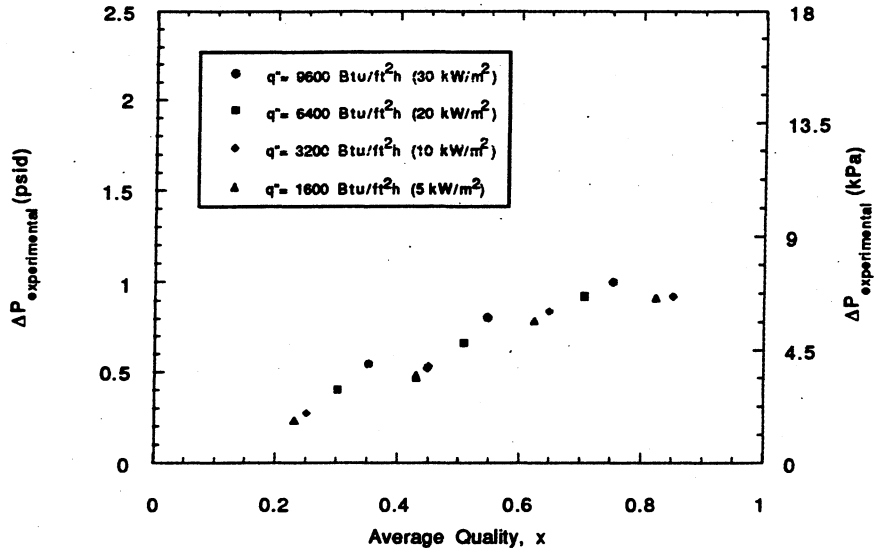

Figure 5.16 Experimental pressure drop versus average quality at G=220 x 10^3 Btu/ft^2-h (300 kg/m^2-s)

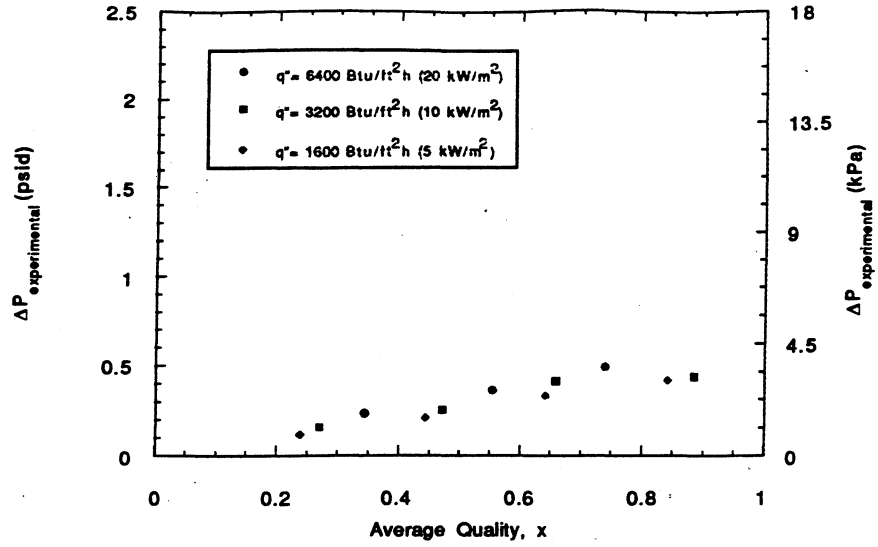

Figure 5.17 Experimental pressure drop versus average quality at G=150 x 10^3 Btu/ft^2-h (200 kg/m^2-s)

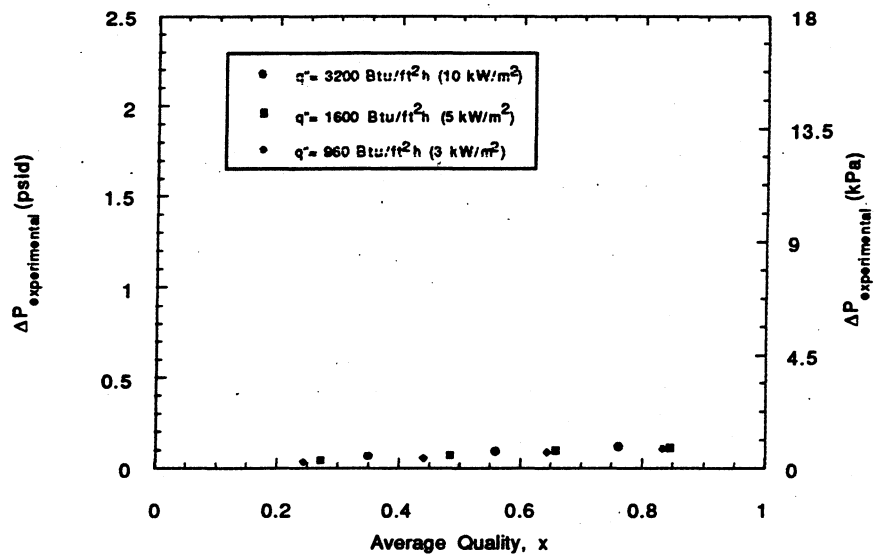

Figure 5.18 Experimental pressure drop versus average quality at G=75 x 10^3 Btu/ft^2-h (100 kg/m^2-s)

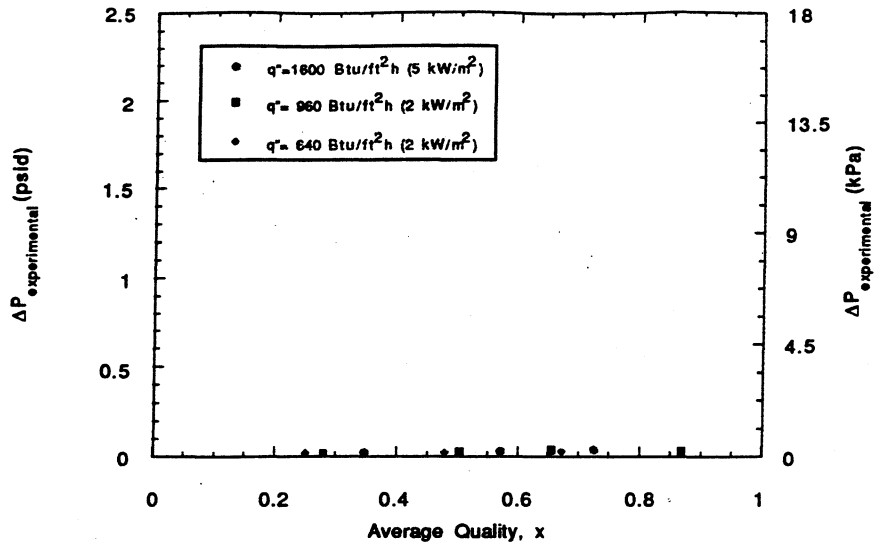

Figure 5.19 Experimental pressure drop versus average quality at G=37 x 10^3 Btu/ft^2-h (50 kg/m^2-s)

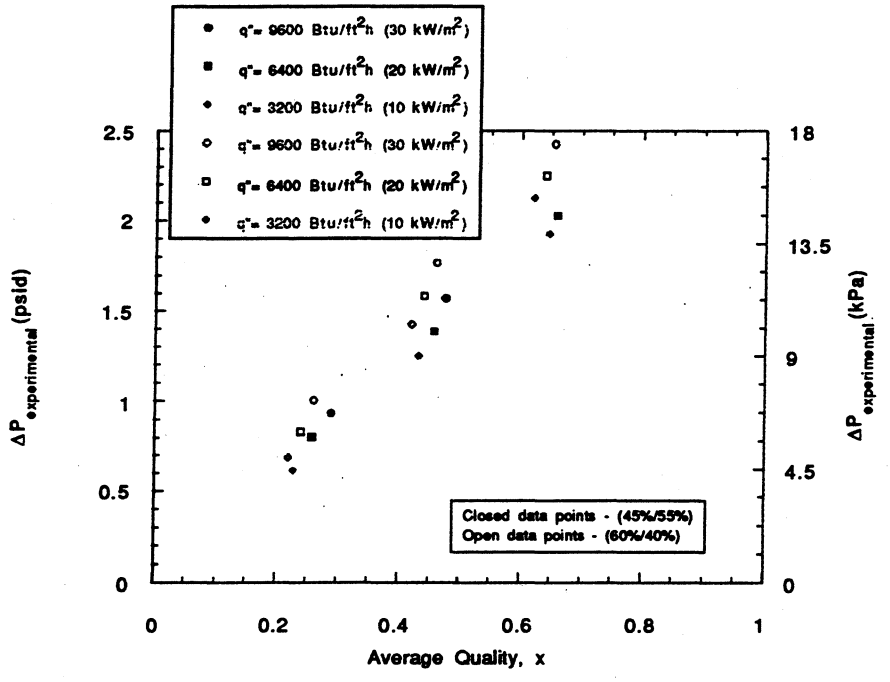

Figure 5.20 Comparison of experimental pressure drop to Christoffersen's [1993] pressure drop at G=370 x 10^3 Btu/ft^2-h (500 kg/m^2-s)

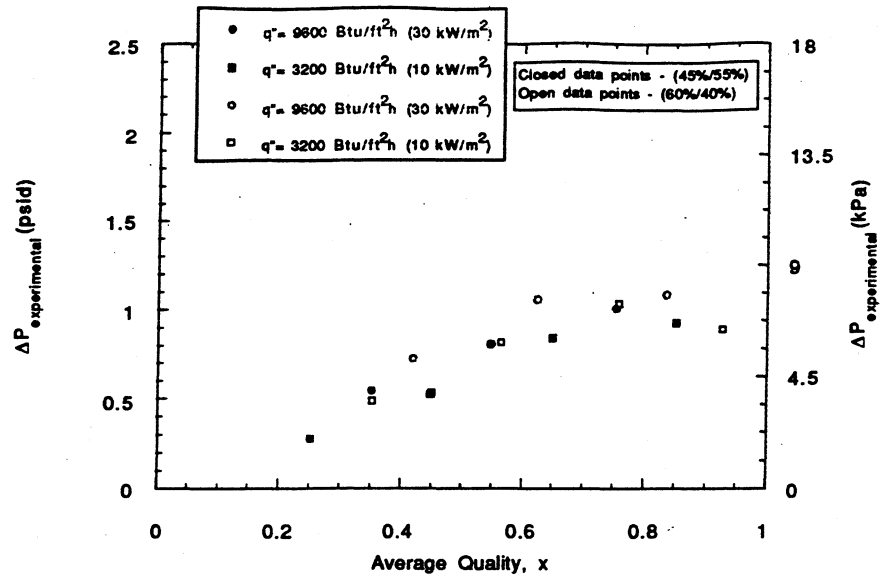

Figure 5.21 Comparison of experimental pressure drop to Christoffersen's [1993] pressure drop at G=220 x 10^3 Btu/ft^2-h (300 kg/m^2-s)

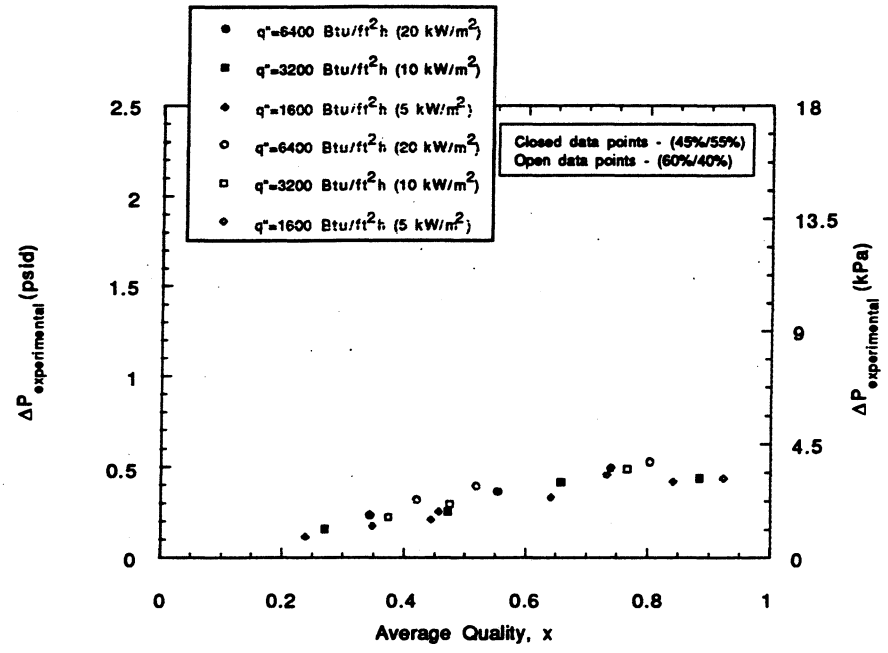

Figure 5.22 Comparison of experimental pressure drop to Christoffersen's [1993] pressure drop at G=150 x 10^3 Btu/ft^2-h (200 kg/m^2-s)

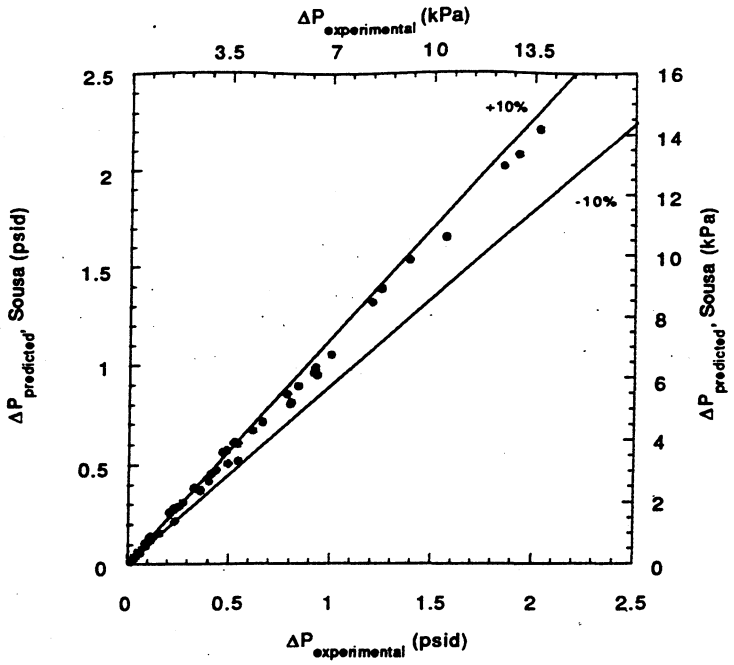

Figure 5.23 Experimental pressure drop versus pressure drop predicted by the Sousa correlation

CHAPTER 6
Conclusions and Recommendations

The goal of this work is to study the heat transfer and pressure drop characteristics of a 45/55 % by weight mixture of R32/R125. Experimental data were gathered and the results were compared to correlations from literature as well as previous R32/R125 data. The following section highlights the main conclusions drawn from the study. This is followed by suggestions for future work.

6.1 Conclusions

When the flow is in the annular regime and the heat flux is low, both the convective and nucleate modes of heat transfer are important. This is shown by a dependence on heat flux and quality. However, as the heat flux is raised, the convective component is suppressed and the Nusselt number becomes independent of quality. If the quality is raised beyond a certain point, which varies with mass flux, the nucleate boiling contribution is suppressed and there is no longer any dependence on heat flux. For low mass fluxes, the flow is in the wavy or stratified regime. The Nusselt numbers are independent of quality for all the conditions and change only with heat flux. Thus, nucleate boiling is the dominant form of heat transfer. At the high heat fluxes, dry out occurs at qualities above 80%.

The experimental data are compared to experimental results gathered by Christoffersen [1993] as well as to correlations by Shah [1976], Jung and Radermacher [1989], and Wattelet [1994]. In Christoffersen's [1993] study, a 60/40 % by weight mixture of R32/R125 was used. Despite this difference, and a slight difference in the temperature glide, the data agree closely. Before any comparisons to the correlations were performed, property data were obtained through two different methods. The first uses curve fits derived from data provided by DuPont. The second method used ideal mixing rules to combine the properties of pure R32 and pure R125. Shah's [1976] correlation, using the DuPont properties, underpredicted the data and most of the points fell within -20% and -40% of the experimental value. The ideal mixture properties slightly decreased the accuracy of the correlation. This discrepancy is attributed to an underestimation of the convective contribution of evaporative heat transfer. Conversely, the Jung and Radermacher [1989] correlation greatly overpredicted the experimental data. This was true using both methods to calculate the properties needed. The lack of accuracy is attributed to lack of accurate surface tension data for the mixture. Finally, the Wattelet [1994] correlation was used to predict the experimental data. Using the properties provided by

DuPont, all the points fall within ± 20%, with most of the data falling within ±10%. Using the ideal mixture data, however, caused an the correlation to overpredict the data.

In addition to the heat transfer data, pressure drop data is also presented. The pressure drop is dependent on mass flux, heat flux, and quality. An increase in any of these parameters causes an increase in the pressure drop. The frictional pressure drop is greatly influenced by the velocity of the vapor phase; thus, it is dependent on both the mass flux and the quality. The acceleration pressure drop is a function of mass flux and the inlet and outlet qualities. Since the change in quality increases as the heat flux increases, the acceleration pressure drop also increases with increasing heat flux.

As with the experimental Nusselt numbers, the experimental pressure drop is also compared to Christoffersen's [1993] data and a two-phase correlation. There is very close agreement between the results of the Christoffersen [1993] study and the present one. There is also very close agreement between the experimental data and the Sousa [1993] correlation. All the points fall within ±10% of the predicted value.

6.2 Recommendations

The results gathered in this study should be used as a baseline for future tests. One set of tests should be an investigation of the effect of small amounts of oil on the heat transfer and pressure drop characteristics of the mixture. Since most refrigeration systems use oil in the compressor, this data would be useful. In addition to the effect of oil, the effect of different geometries should also be researched. Currently, there is great interest in using flat plate evaporators in automotive cooling systems. How the heat transfer and pressure drop change with this new configuration would be of great interest to the automobile industry. Additionally, internally enhanced tubes are becoming more prevalent. The behavior of the R32/R125 mixture in these tubes should be investigated. This study should be done with and without oil and with different internal fin configurations.

REFERENCES

Altman, M., T. H. Norris, and F. W. Staub, "Local and average heat transfer and pressure drop for refrigerants evaporating in horizontal tubes," Journal of Heat Transfer, ASME, 189-198, 1960

Bird, R. B., W. E. Stewart, and E. N. Lightfoot, *Transport phenomena,* John Wiley & Sons, Inc., New York, 1960

Carey, V. P., *Liquid-vapor Phase Change Phenomena*, Hemisphere, New York, 1992

Celata, G. P., Aimo, M., and Setaro, T., "Forced convective boiling in binary mixtures", International Journal of Heat and Mass Transfer, 36(13), 3299-3309, 1993

Cooper, M. G., "Saturation pool boiling - A simple correlation," International Chemical Engineering Symposium series, 86,785-792,1984

Christofersen, B. C., "Heat transfer and flow characteristics of R-22, R-32/R-125, and R-134a in smooth and micro-fin tubes," M.S. thesis, University of Illinois at Urbana-Champaign, 1993

Dittus, F.W. and L. M. K. Boelter, University of California Publications on Engineering, 2, 443, 1930

Dobson, M., "Heat transfer and flow regimes during condensation in horizontal tubes", Ph.D. Dissertation, University of Illinois, 1994

Dobson, M. K., J. C. Chato, and et al., "Heat transfer and flow regimes during condensation in horizontal tubes," ACRC TR-57, May 1994

Gnielinski, V., "New equations for heat and mass transfer in turbulent pipe and channel flow," International Chemical Engineering , 16, 359-368, 1976

Jung, D. S., M. McLinden, R. Radermacher, and D. Didion, "A study of flow boiling heat transfer with refrigerant mixtures," International Journal of Heat and Mass Transfer, 32(9), 1751-1764, 1989

Jung, D. and R. Radermacher, "Transport properties and surface tension of pure and mixed refrigerants," ASHRAE Transactions, 97(1), 90-99, 1990

Jung, D. and R. Radermacher, "Prediction of evaporation heat transfer coefficient and pressure drop of refrigerant mixtures in horizontal tubes," Revue Practique du Froid et du Conditionment D'air, 16(3), 201-209, 1993

Kedzierski, M. A., J. H. Kim, and K. A. Didion, "Cause of the apparent heat transfer degradation for refrigerant mixtures," HTD v. 197, Two-Phase Flow and Heat Transfer, ASME, 149-158, 1992

Kutateladze, S. S., "Boiling heat transfer," International Journal of Heat and Mass Transfer, 4, 3-45, 1961

Lockhart, R. W. and R. C. Martinelli, "Proposed correlation of data for isothermal two-phase, two component flow in pipes," Chemical Engineering Progress, 45(1), 39-48, 1947

Moffat, R.J., "Describing the uncertainties in experimental results," Experimental Thermal and Fluid Science 1, 3-17, 1988

Panek, J. S., "Evaporation heat transfer and pressure drop in ozone-safe refrigerants and refrigerant-oil mixtures," M.S. thesis, University of Illinois at Urbana-Champaign, 1992

Petukhov, B. S., *Advances in Heat Transfer*, Academic, New York, 6, 503-564, 1970

Ross, H., R. Radermacher, M. Di Marzo, and D. Didion, "Horizontal flow boiling of pure and mixed refrigerants," Journal of Heat and Mass Transfer, 30(5), 979-992, 1987

Sami, S. M., J. Schnotale, and J. G. Smale, "Prediction of the heat transfer characteristics of R-22/R-152a/R-114 and R-22/R-152a/R124," ASHRAE Transactions, 98(2), 51-58, 1992

Sardesai, R. G., R. A. W. Shock, and D. Butterworth, "Heat and mass transfer in multicomponent condensation and boiling," Heat Transfer Engineering, 3(3-4), 104-114, 1982

Shah, M. M., "A new correlation for heat transfer during boiling flow through pipes," ASHRAE Transactions, 82(2), 66-86, 1976

Shock, R. A. W., "Nucleate boiling in binary mixtures," International Journal of Heat and Mass Transfer, 20, 701-709, 1977

Sousa, A. L., J. C. Chato, and J. P. Wattelet, "Pressure drop during two-phase flow of refrigerants in horizontal smooth tubes," ACRC-TR-25, 1992

Sousa, A. L., J. C. Chato, J. M. S. Jabardo, J. P. Wattelet, J. Panek, B. Christoffersen, and N. Rhines, "Pressure drop during two-phase flow of refrigerants in horizontal smooth tubes," National Heat Transfer Conference, 1993 (submitted and approved)

Stephan, K. and M. Andelsalam, "Heat transfer correlations for natural convection boiling," International Journal of Heat and Mass Transfer, 23, 73-87, 1980

Stephan, K., "Two-phase heat exchange for new refrigerants and their mixtures," International Journal of Refrigeration, 18(3), 198-209, 1995

Thome, J. R., "Prediction of binary mixture boiling heat transfer coefficients using only phase equilibrium data," International Journal of Heat and Mass Transfer, 26(7), 965-974, 1983

Thome, J. R., and R. A. W. Shock, "Boiling multicomponent liquid mixtures," Advances in Heat Transfer, 16, 59-157, 1984

Unal, H. C., "Prediction of nucleate pool boiling heat transfer coefficients for binary mixtures," International Journal of Heat and Mass Transfer, 29(4), 637-640, 1986

Wattelet, J. P., "Design, building, and baseline testing of an apparatus used to measure evaporation characteristics of ozone-safe refrigerants," M.S. thesis, University of Illinois at Urbana-Champaign, 1990

Wattelet, J. P., J. C. Chato, et al., "Heat transfer flow regimes of refrigerants in a horizontal-tube evaporator," ACRC TR-55, May 1994

Wattelet, J. P., J. C. Chato, et al., "Evaporative characteristics of R-12, R-134a, and MP-39 at low mass fluxes," ASHRAE Transactions, 100(1), 603-615, 1994

Wattelet, J. P., "Heat transfer flow regimes of refrigerants in a horizontal-tube evaporator," Ph.D. Thesis, University of Illinois at Urbana-Champaign, 1994

Zivi, S. M., "Estimation of steady-state steam void fraction by means of the principle of minimum entropy generation," Journal o f Heat Transfer, 86, 247-252, 1964

APPENDIX A
Thermophysical Properties

Property curve fits used in this study are generated from data provided by DuPont. All the curve fits are in SI units. The different properties and their respective units are as follows:

T	Temperature	℃
P	Pressure	kPa
i_l	Liquid enthalpy	kJ/kg
i_v	Vapor enthalpy	kJ/kg
i_{lv}	Enthalpy of vaporization	kJ/kg
ρ_l	Liquid density	kg/m^3
ρ_v	Vapor density	kg/m^3
Cp_l	Liquid specific heat	kJ/kg-°C
k_l	Liquid thermal conductivity	mW/m-°C
μ_l	Liquid viscosity	μPa-s
μ_v	Vapor viscosity	μPa-s

Curve Fits

$$T_{sat} = -6.033e^{-12}P^4 + 3.819e^{-8}P^3 - 9.276e^{-5}P^2 + 0.127P - 58.335$$

$$P_{sat} = 3.860e^{-6}T^4 + 1.647e^{-3}T^3 + 0.304T^2 + 25.206T + 791.882$$

$$i_l = -7.776e^{-12}P^4 + 4.940e^{-8}P^3 - 1.202e^{-4}P^2 + 0.172P + 118.254$$

$$i_l = 1.459e^{-5}T^3 + 2.401e^{-3}4T^2 + 1.488T + 199.971$$

$$i_v = -2.268e^{-7}T^4 - 2.461e^{-5}T^3 - 3.292e^{3}T^2 + 0.3067T + 415.352$$

$$i_{lv} = 4.192e^{-12}P^4 - 2.697e^{-8}P^3 + 6.600e^{-5}P^2 - 0.109P + 271.810$$

$$i_{lv} = -3.644e^{-7}T^4 - 3.894e^{-5}T^3 - 5.500e^{-3}T^2 - 1.182T + 215.350$$

$$\rho_l = 2.031e^{-6}T^4 - 1.393e^{-4}T^3 - 0.018T^2 - 4.084T + 1186.554$$

$$\rho_v = 1.240e^{-6}T^4 + 1.404e^{-4}T^3 + 0.137T^2 + 1.008T + 31.470$$

$$Cp_l = 7.420e^{-13}T^7 - 1.378e^{-11}T^6 - 1955e^{-9}T^5 + 4.206e^{-8}T^4 + 2.408e^{-6}T^3 + 5.475e^{-5}T^2 + 6.284e^{-3}T + 1.611$$

$$k_l = -1.29e^{-5}T^3 + 6.86e^{-4}T^2 - 0.471T + 100.1$$

$$\mu_l = -9.2e^{-5}T^3 + 1.81e^{-2}T^2 - 2.25T + 1.66$$

$$\mu_v = 3.98e^{-2}T + 11.7$$

APPENDIX B
Experimental Data

Table B.1 presents the experimental data obtained in this study. The column headings and their respective units are as follows:

T	Inlet temperature	℃
G	Mass flux	kg/m^2-s
q"	Heat flux	kW/m^2
x_{avg}	Average quality	
h	Heat transfer coefficient	W/m^2-K
Nu	Nusselt number	
δh	Percent uncertainty	
ΔP	Pressure drop	kPa

Table B.1 Experimental data

T	G	q"	x_{avg}	h	Nu	δh	ΔP
4.8	502	20	0.6595	6443	510.24	9.00	14.00
4.8	500	10	0.6456	6220	492.70	17.47	13.29
4.8	501	5	0.6328	6362	503.90	34.23	12.78
4.9	503	30	0.4761	6787	537.80	6.60	10.81
4.9	504	20	0.4573	5925	469.43	8.53	9.55
4.9	503	10	0.4327	5042	399.58	14.37	8.59
4.9	504	5	0.4197	4826	382.49	27.80	8.27
5.0	500	30	0.2901	6842	542.28	6.58	6.42
5.1	503	20	0.2592	5698	451.86	8.24	5.52
5.0	505	10	0.2291	4312	341.80	12.36	4.25
5.0	506	5	0.2143	3781	299.72	22.12	3.75
5.0	300	10	0.8517	4807	381.04	13.45	6.35
4.9	299	5	0.8245	4734	375.20	27.25	6.29
4.9	300	30	0.7537	6728	533.21	6.44	6.89
4.9	300	20	0.7064	5643	447.19	8.17	6.36
4.9	305	10	0.6498	4767	377.72	13.57	5.78
5.0	307	5	0.6248	4360	345.59	25.08	5.41
5.0	301	30	0.5476	6588	522.23	6.36	5.55
5.1	299	20	0.5086	5491	435.44	7.99	4.58
5.1	304	10	0.4503	4222	334.77	12.19	3.68
5.0	304	10	0.4492	4019	318.59	11.69	3.61
5.0	303	5	0.4306	3456	274.03	20.19	3.24
5.0	306	5	0.4300	3590	284.60	20.92	3.35
5.0	304	30	0.3524	6510	516.12	6.33	3.76
5.1	307	20	0.3024	5475	434.15	7.97	2.77
5.0	302	10	0.2521	4252	337.15	12.36	1.90
5.0	306	5	0.2316	3256	258.17	19.10	1.60
5.0	198	10	0.8856	3943	312.57	11.53	3.02
5.0	198	5	0.8423	3682	291.96	21.69	2.89
5.0	205	20	0.7400	5450	432.00	7.85	3.40
5.0	211	10	0.6587	3937	312.10	11.63	2.85
5.0	199	5	0.6423	3222	255.45	18.91	2.29
5.1	202	20	0.5539	4517	358.20	6.69	2.50
5.0	202	10	0.4715	3356	266.08	10.13	1.75
5.1	201	5	0.4440	2637	209.10	16.07	1.44
5.1	200	20	0.3446	4783	379.31	7.00	1.62
5.1	204	10	0.2704	3569	283.00	10.61	1.09
5.1	199	5	0.2397	2481	196.73	15.38	0.80
5.2	104	5	0.8461	1547	122.74	11.18	0.78
5.1	103	3	0.8337	1535	121.75	18.57	0.74
5.2	99	10	0.7612	2573	204.20	7.67	0.82
5.1	103	5	0.6581	2134	169.29	13.92	0.66
5.0	102	3	0.6437	1691	134.05	19.35	0.61
5.1	100	10	0.5586	3245	257.43	9.72	0.65
5.1	101	5	0.4838	2207	175.09	14.05	0.49
5.1	101	3	0.4400	1641	130.19	19.35	0.37

Table B.1 Experimental data

T	G	q"	x_{avg}	h	Nu	δh	ΔP
5.2	102	10	0.3496	3113	247.03	9.45	0.45
5.0	103	5	0.2722	2094	166.04	13.81	0.29
5.0	104	3	0.2436	1524	120.80	18.48	0.22
5.1	53	5	0.7263	1856	147.19	12.30	0.25
5.0	54	3	0.6559	1613	127.90	18.24	0.25
5.0	50	2	0.6730	1221	96.76	24.13	0.19
5.1	48	5	0.5716	2108	167.14	13.66	0.20
5.0	49	3	0.5039	1670	132.45	19.09	0.17
5.0	49	2	0.4789	1287	102.02	25.23	0.16
5.1	50	5	0.3480	2202	174.63	13.99	0.15
5.0	51	3	0.2808	1539	122.01	18.57	0.12
4.9	53	2	0.2508	1213	96.11	23.79	0.12
5.2	50	3	0.8689	1161	92.10	15.30	0.22